Science of the Total Environment 905 (2023) 167038

Contents lists available at ScienceDirect

Science of the Total Environment

journal homepage: www.elsevier.com/locate/scitotenv

Emissions from modern engines induce distinct effects in human olfactory mucosa cells, depending on fuel and aftertreatment

Laura Mussalo [a], Simone Avesani [b], Muhammad Ali Shahbaz [a], Táňa Závodná [c], Liudmila Saveleva [a], Anssi Järvinen [d], Riikka Lampinen [a], Irina Belaya [a], Zdeněk Krejčík [c], Mariia Ivanova [a], Henri Hakkarainen [e], Juho Kalapudas [f], Elina Penttilä [g], Heikki Löppönen [g], Anne M. Koivisto [f,h,i], Tarja Malm [a], Jan Topinka [c], Rosalba Giugno [b], Päivi Aakko-Saksa [d], Sweelin Chew [a], Topi Rönkkö [j], Pasi Jalava [e], Katja M. Kanninen [a,*]

[a] A. I. Virtanen Institute for Molecular Sciences, University of Eastern Finland, 70210 Kuopio, Finland
[b] Department of Computer Science, University of Verona, 37134 Verona, Italy
[c] Department of Genetic Toxicology and Epigenetics, Institute of Experimental Medicine of the Czech Academy of Sciences, Videnska 1083, 142 20 Prague, Czech Republic
[d] VTT Technical Research Centre of Finland, VTT, 02044 Espoo, Finland
[e] Inhalation Toxicology Laboratory, Department of Environmental and Biological Sciences, University of Eastern Finland, 70211 Kuopio, Finland
[f] Department of Neurology, Neuro Centre, Kuopio University Hospital, 70210 Kuopio, Finland
[g] Department of Otorhinolaryngology, University of Eastern Finland and Kuopio University Hospital, 70210 Kuopio, Finland
[h] Brain Research Unit, Department of Neurology, School of Medicine, University of Eastern Finland, 70210 Kuopio, Finland
[i] Department of Neurology and Geriatrics, Helsinki University Hospital and Neurosciences, Faculty of Medicine, University of Helsinki, 00014 Helsinki, Finland
[j] Aerosol Physics Laboratory, Physics Unit, Tampere University, 33014 Tampere, Finland

HIGHLIGHTS

- Olfactory mucosa (OM) cells: a relevant model to study effects of air pollution
- Emission characterization data combined with gene-level alterations in OM cells
- UFPs might mediate harmful effects on the brain through the olfactory route.
- Fossil diesel causes more severe adverse effects than renewable diesel.
- PAHs may disturb inflammatory processes and xenobiotic metabolism in OM cells.

GRAPHICAL ABSTRACT

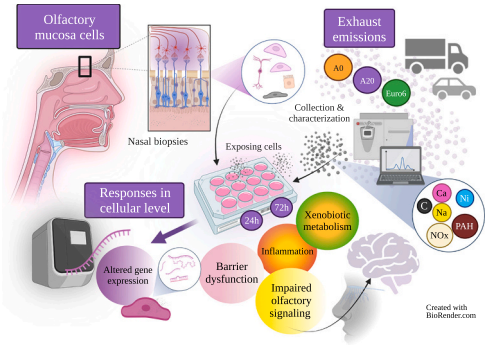

ARTICLE INFO

Editor: Anastasia Paschalidou

ABSTRACT

Ultrafine particles (UFP) with a diameter of ≤0.1 μm, are contributors to ambient air pollution and derived mainly from traffic emissions, yet their health effects remain poorly characterized. The olfactory mucosa (OM) is located at the rooftop of the nasal cavity and directly exposed to both the environment and the brain. Mounting

Abbreviations: OM, olfactory mucosa; UFP, ultrafine particles; PAH, polycyclic aromatic hydrocarbons.

* Corresponding author.
E-mail address: katja.kanninen@uef.fi (K.M. Kanninen).

https://doi.org/10.1016/j.scitotenv.2023.167038
Received 16 June 2023; Received in revised form 30 August 2023; Accepted 11 September 2023
Available online 13 September 2023

Keywords:
Air pollution
Traffic emissions
Ultrafine particles (UFP)
RNA-Seq

evidence suggests that pollutant particles affect the brain through the olfactory tract, however, the exact cellular mechanisms of how the OM responds to air pollutants remain poorly known. Here we show that the responses of primary human OM cells are altered upon exposure to UFPs and that different fuels and engines elicit different adverse effects. We used UFPs collected from exhausts of a heavy-duty-engine run with renewable diesel (A0) and fossil diesel (A20), and from a modern diesel vehicle run with renewable diesel (Euro6) and compared their health effects on the OM cells by assessing cellular processes on the functional and transcriptomic levels. Quantification revealed all samples as UFPs with the majority of particles being $\leq$0.1 μm by an aerodynamic diameter. Exposure to A0 and A20 induced substantial alterations in processes associated with inflammatory response, xenobiotic metabolism, olfactory signaling, and epithelial integrity. Euro6 caused only negligible changes, demonstrating the efficacy of aftertreatment devices. Furthermore, when compared to A20, A0 elicited less pronounced effects on OM cells, suggesting renewable diesel induces less adverse effects in OM cells. Prior studies and these results suggest that PAHs may disturb the inflammatory process and xenobiotic metabolism in the OM and that UFPs might mediate harmful effects on the brain through the olfactory route. This study provides important information on the adverse effects of UFPs in a human-based *in vitro* model, therefore providing new insight to form the basis for mitigation and preventive actions against the possible toxicological impairments caused by UFP exposure.

1. Introduction

Air pollution is a major global health risk estimated to cause yearly millions of deaths and the loss of healthy years of life (World Health Organization, 2021). A large literature on epidemiological and experimental studies has shown that air pollution is harmful to health and exposure to particulate matter (PM) is mainly associated with diseases of the cardiovascular and respiratory systems (Fuzzi et al., 2015). A growing body of evidence suggests that the neurological system is also targeted by air pollution, especially by particulate compounds in smaller particle size fractions (Hahad et al., 2020). The association between PM and cognitive decline as well as other neurological effects is documented (Calderón-Garcidueñas et al., 2021; Iaccarino et al., 2021; Jew et al., 2019; Zundel et al., 2022). Particles are thought to reach the brain either through the bloodstream or directly via the olfactory nerve, which is connected to the olfactory mucosa (OM) located at the rooftop of the nasal cavity (Costa et al., 2020; Hochella et al., 2019; Jankowska-Kieltyka et al., 2021; Maher et al., 2016; Schraufnagel, 2020).

Air quality is monitored by measuring different compounds and particles in the air, e.g., nitrogen oxides (NO_x), sulfur dioxide (SO_2), ozone (O_3), and particulate matter with a diameter of smaller than 10 μm (PM_{10}) and smaller than 2.5 μm ($PM_{2.5}$) (Hahad et al., 2020; World Health Organization, 2021). Measurements of PM_{10} have been conducted for over two decades in Europe, and later the air quality guidelines have also included $PM_{2.5}$. Still, yet to this day, less attention has been paid to ultrafine particles (UFP) with a diameter of 0.1 μm or less (Cassee et al., 2019; Fuzzi et al., 2015; Nazarenko et al., 2021; Rönkkö and Timonen, 2019). Although UFPs were acknowledged in the newest WHO Air Quality guideline report published in 2021, it was stated that there is not enough epidemiological evidence to set concrete air quality guidelines for UFPs. Therefore, more experimental and epidemiological studies of the adverse effects of UFP exposure are desperately needed.

The biggest anthropogenic sources of UFPs of ambient air are combustion-based processes that utilize fossil fuels and biofuels, including exhaust from vehicle engines and biomass burning (Kwon et al., 2020; Rönkkö and Timonen, 2019; World Health Organization, 2021). Advances in exhaust aftertreatment technologies have led to reduced amounts of solid particle emissions, resulting in better-measured air quality in many large cities (Kwon et al., 2020; Luoma et al., 2021; Steiner et al., 2016). However, several types of gaseous compounds may pass through the filtration systems, potentially leading to the formation of particles in the atmosphere; UFPs can be formed from semivolatile compounds that pass the exhaust aftertreatment systems or even form in those systems (Kwon et al., 2020).

The nasal cavity works as an entrance hall where inhaled air is assessed, pre-processed (warming and moisturizing), and guided forward to the lungs where gas exchange occurs (Freeman et al., 2021). The olfactory mucosa (OM), located at the rooftop of the nasal cavity, consists of epithelium, basement membrane, and lamina propria, which are specialized in odor perception (Chen et al., 2014). Increasing evidence of its dysfunction as an early marker for neuropathogenesis presents an avenue for in-depth exploration of its role in how the brain deals with environmental exposures such as air pollution (Kanninen et al., 2020). The exact means by which the OM responds to air pollutants remains to be fully elucidated, although previous work with a primary human OM cell culture model revealed mitochondrial dysfunction, inflammation, and apoptotic features when cultures were exposed to PM collected from an urban environment in China (Chew et al., 2020). Toxicogenomic studies with primary human nasal epithelial cells have also revealed a biological relationship between epithelial damage and exposure to diesel exhaust particles (Kim et al., 2020a). However, little is known about the detailed cellular and molecular mechanisms caused by UFPs on OM cells. Based on previous work it is known that the primary human OM cultures are heterogenous, similar to in vivo, including but not limited to the epithelial cells (Chew et al., 2020; Lampinen et al., 2022). Given that the OM can be a gateway of particles to the brain, it is important to focus research efforts on uncovering how environmental insults exploit this path to the detriment of the brain. A recent review summarizes how exposure to $PM_{2.5}$ or other air pollutants (e.g., traffic-related emissions) is associated with neuroinflammation due to their transition to the brain through the olfactory route (Cristaldi et al., 2022). Altered expression of genes mediating olfactory dysfunction in the olfactory epithelium (OE) of mice exposed to diesel exhaust particles has also been reported (Kim et al., 2020b). Despite many animal studies linking OM as a gateway of pollutants to the brain, anatomical differences between species must be considered when applying findings to humans (Kanninen et al., 2020). In support of this, a stronger response to polycyclic aromatic hydrocarbons (PAH) has been reported in human cells when compared to rodents (Vondracek et al., 2017).

Here, we utilize a highly translational primary cell model of the OM (Lampinen et al., 2022) to investigate cellular and molecular mechanisms occurring upon exposure to traffic-related UFPs. We harness state-of-the-art methods for the characterization of UFPs and combine this information with multiple layers of data and information collected from human cells. For the first time, different aftertreatment systems and fuels are compared on the transcriptomic level in OM cells by RNA-sequencing (RNA-Seq).

2. Materials and methods

2.1. Cell culture

Primary OM cell cultures from $n = 8$ donors were established as described in detail by (Lampinen et al., 2022). This work has received approval for research ethics from the Research Ethics Committee of the Northern Savo Hospital District (permit number 536/2017). Written

informed consent was obtained from all the donors. In brief, OM biopsies were received via the Department of Otorhinolaryngology, Kuopio University hospital from patients undergoing a dacryocystorhinostomy (DCR) surgery. Biopsy of the OM was taken from the nasal septum close to the rooftop of the nasal cavity and immediately transferred on ice to the laboratory where the tissue piece was processed mechanically and enzymatically to obtain dissociated single cells. Cell cultures were expanded, and cells were banked to liquid nitrogen. Used OM cells were primary lines between passages 5 and 7. Cells were cultured as submerged cultures in Dulbecco's Modified Eagle Medium: Nutrient Mixture F12 (DMEM/F-12) (Gibco #11320-033) containing 10 % heat-inactivated Fetal Bovine Serum (Gibco #10500-064) and 1 % of Penicillin-Streptomycin (10,000 U/ml) (Gibco #15140-122) at humified conditions at 37 °C, 5 % CO_2. For experiments, cells were plated with varying densities depending on the experiment performed two-three days before exposures to allow them to adhere and divide.

2.2. Air Liquid Interface (ALI) cultures

OM cell line of passage 3 was cultured as submerged culture until reaching 70 % confluence. Cells were harvested and seeded with a density of 50,000 cells to tissue culture insert for 24-well (0,4 μm, transparent) (Sarstedt #83.3932.041), coated with 1:100 Matrigel Growth Factor Reduced (GFR) Basement Membrane Matrix (Corning #356231). Full medium changes in both the basal and apical chambers were done every two days until confluence was reached. At the start of an Air Liquid Interface (ALI) culture, the medium from the apical side was removed and the medium from the basal compartment was replaced by ALI-medium, composed of Pneumacult-ALI medium kit (STEMCELL Technologies #5001), Hydrocortisone Stock Solution (STEMCELL Technologies #7925), Heparin Solution (Parano LEO 5000 IU/ML) and Penicillin-Streptomycin (10,000 U/ml) (Gibco #15140122). Complete medium change was performed every two days for four weeks until the exposures to A0, A20, and Euro6.

2.3. UFP sample collection and characterization

The particle samples were collected by VTT Technical Research Centre of Finland from the exhaust of a heavy-duty diesel engine, abbreviated herein as 'HDE' and a 2019 model diesel vehicle, abbreviated herein as 'DI-E6d'. The HDE was a modern 4-cylinder 4.4 dm^3 turbocharged diesel unit equipped with high-pressure common-rail fuel injection. As an important factor for the interpretation of the results, it's clarified that the HDE was not equipped with any exhaust aftertreatment devices. Thus, the collected samples represent engine-out emissions. The DI-E6d was a modern diesel passenger car with a 1.6 dm^3 turbocharged engine and Euro 6d-temp emission rating. The exhaust aftertreatment consisted of a Diesel Particulate Filter (DPF) to reduce particle emissions and a Selective Catalytic Reduction (SCR) to reduce NO_x emissions.

The engine was run in an electrical dynamometer measuring the power and the torque according to ISO 8178 RMC-C1 test cycle, which consists of 2-5 min constant modes with certain engine speed and torque and linear ramps with a duration of 20 s between these modes. The vehicle was driven on the VTT light-duty chassis dynamometer according to the Worldwide harmonized Light duty Test Cycle (WLTC).

The engine was run with two fuels: regular fossil diesel (in this paper A20) and paraffinic renewable diesel (Neste renewable diesel, in this paper A0). The regular fossil diesel met the EN590 specifications, the total aromatic content was 20 wt% (percentage by weight), and Fatty Acid Methyl Ester (FAME) content was <0.1 vol% (percentage by volume). The renewable diesel was Hydrotreated Vegetable Oil (HVO)-type fuel made of renewable feedstocks with 0.1 wt% of total aromatics and the FAME content was <0.1 vol%. The main difference between the renewable diesel compared to biodiesel is the production which uses the catalytic hydro-processing method, while biodiesel or FAME is produced via transesterification (*Neste Renewable Diesel Handbook*, 2020; Xu et al., 2022). Unlike traditional biodiesel, the new generation renewable diesel can be used as the sole fuel in engines due to fuel quality even better than the fossil diesel. Both fuels were supplied by the same refining company (Neste Oyj, Espoo, Finland) and were analyzed in an external laboratory (ASG Analytik-Service GmbH, Neusäss, Germany). In the case of the HDE, the filter samples were collected from the raw exhaust with a diluting sampling system (SPC472 Smart Sampler, AVL List GmbH, Graz, Austria) according to ISO 8178 standard.

The dilution ratio was set to 6 and the total flow of diluted exhaust through the filter was 70 l/min. Two parallel filter holders were used simultaneously, with a primary filter and a backup filter in both filter holders. Particles used for this study were collected on primary pre-treated fluorocarbon membrane filters, 70 mm (o.d.; optical density) (Fluoropore, Merck KGaA, Darmstadt, Germany). The backup filters were placed in the filter holders, but they were not extracted for biological analyses.

Exhaust from the tailpipe of the DI-E6d car was led to a Constant Volume Sampler (CVS)-type dilution tunnel as in standard emissions measurements. In the tunnel, a sample was diluted with HEPA-filtered air with a variable dilution ratio depending on the exhaust flow. The dilution ratio was 6-8, on average. The total flow of diluted exhaust through the filter was 100 l/min. Two parallel filter holders were used simultaneously. Particles used for this study were collected on primary pre-treated fluorocarbon membrane filters, 70 mm (o.d.) (Fluoropore, Merck KGaA, Darmstadt, Germany).

Before collection on filters, filter material (MerckMillipore, Fluoropore) was washed with HPLC-grade methanol three times, dried, and weighed. The filters for the collection were stored on individual Petri dishes, closed to prevent contaminations. After the collection, filters were weighed and stored at −20 °C before extraction procedures.

2.4. Filter extraction of exposure material

Before extraction, filters were weighed with an analytical balance to calculate the collected mass. For extraction, filters were cut into four pieces and placed into a 50 ml glass tube, which was filled with HPLC-grade methanol, and sonicated for 30 min at a temperature <30 °C. Thereafter, the methanol suspensions from all of the filters from the same sample were transferred to a rotary evaporator flask. This procedure was repeated twice for each filter. After the extraction, the sample was reduced to a small volume in a rotary evaporator, set at 35 °C and 150 mbar. This small volume was measured, and transferred into 15 ml glass vials, based on calculated emission volumes and collected mass. The methanol in each vial was evaporated under nitrogen flow and thereafter the remaining dry samples were stored at −20 °C until the cell exposures. All the same procedures, except for actual sample collection, were conducted for blank control filters.

2.5. UFP exposures

Pollutant particles were suspended in 10 % *v*/v sterile Dimethylsulfoxide (DMSO) (Sigma-Aldrich #D2650) in sterile water (Baxter) and sonicated in an ultrasonic water bath for 30 min. Prior to the exposure, to ensure a homogenous mixture, samples were either mixed thoroughly by pipetting or by further sonication for 5 min. The control was prepared by mixing 10 % *v*/v sterile DMSO with sterile water. The final DMSO concentration used on the cells was 0.2 %–2 %. To outrule the effect of DMSO itself, treatments with different concentrations were compared to corresponding control-treated cells. The cell culture media was changed 1 h prior to pollutant exposures. Cells were treated with pollutants in final concentrations of 10, 20, 50, 100, 200, and 400 l/ml in culture media, with concentrations referring to the amount of exhaust run through the collection filter. Rather than using a mass, we used the volume of the exhaust as the dose metric, since mass is known to correlate poorly with the surface area of UFPs (Cassee et al., 2019). With ALI-cultures exposures were executed by adding 60 μl of media

containing UFPs at a concentration of 20 l/ml to the apical compartment. After exposure, cells were kept for either 24-h or 72-h at humidified conditions at 37 °C, 5 % CO_2.

2.6. Measurement of metabolic activity and cytotoxicity

MTT (3-(4.5-dimethylthiazol-2-yl)-2.5-diphenyltetrazolium bromide) tetrazolium reduction assay was used to assess the metabolic activity of exposed cells. Cells were plated on 48-well plates with a density of 20,000 cells/well. Cells were exposed to pollutants for 24-h and 72-h, with four technical replicates per treatment. After the exposure, UFP-containing media was collected and replaced with media containing 1.2 mM Thiazolyl blue tetrazolium bromide (VWR #0793-1G) and incubated for 2.5–3-h at 37 °C. After incubation, the media was removed and the formed crystal-salts were solubilized in DMSO (Fisher Chemical #D/4121/PB15, 67-68-5). The absorbances were measured at 595 nm with a Wallac Victor 1420 plate reader (Perkin Elmer, Waltham, USA), and the background signal (measured with DMSO) was subtracted from readings. All values were normalized to control-treated cells. The collected culture media was used for quantification of lactate dehydrogenase (LDH) release with CyQUANT™ LDH Cytotoxicity Assay Kit (Invitrogen #C20301) and performed according to the manufacturer's instructions. Absorbances were read at 490 nm and 650 nm using the Wallac Victor 1420 plate reader (Perkin Elmer, Waltham, USA). Cells lysed with Triton-X (Sigma-Aldrich #9002-93-1) were used as a positive control for cell death.

2.7. Transcriptomic analysis

RNA-seq was performed on six primary OM cell lines. Cells were plated to 6-well plates at a density of 150,000 cells/well three days prior to exposures. After 24-h and 72-h exposures to A0, A20, and Euro6 at a concentration of 20 l/ml, the culture media was collected, cells were washed with ice-cold Dulbecco's phosphate-buffered saline (D-PBS) (Gibco #14190-094) and RNA was extracted using the protocol provided by the manufacturer of the kit AllPrep DNA/RNA/miRNA (Qiagen #80224), DNase treatment included. The RNA quality was determined using the RNA Pico or Nano 6000 LabChip kit (Agilent Technologies, USA #5067-1513 or #5067-1511). The LabChips were run in an Agilent 2100 Bioanalyzer according to the manufacturer's instructions. Analyses of RNA yield were performed using Qubit. Samples with RNA integrity numbers higher than 6 were selected for sequencing. Ribosomal RNA was depleted using NEBNext® rRNA Depletion Kit v2 (Human/Mouse/Rat) (New England BioLabs). cDNA libraries were prepared using the NEBNext® Ultra™ II Directional RNA Library Prep Kit for Illumina® (New England BioLabs). SPRi beads (Beckman Coulter Inc.) were employed for purification and size selection. Libraries were sequenced as paired-end sequencing on the Illumina NovaSeq 6000 platform using NovaSeq 6000 S1 Reagent Kit v1.5 (200 cycles) (Illumina).

RNA-seq analysis was conducted separately on 24-h and 72-h exposed samples. FastQC tool (Andrews, 2010), used to check the quality of sequenced reads, highlighted the presence of potential adapter sequences that were extracted and trimmed from the reads through the use of the Trimmomatic tool (Bolger et al., 2014). Pre-processed reads were aligned to the human HG38 Gencode indexed genome using STAR tool (v2.4) (Dobin et al., 2013) then, mapped reads were quantified through the featureCounts tool (Liao et al., 2014). Statistical analysis was conducted independently on both expression matrices using the R package DESeq2 (Love et al., 2014). Exploratory analysis revealed in both datasets a batch effect due to the cell line of origin of each sample. Looking at the Principal Component Analysis (PCA) plots we observed that samples were grouped by cell line of origin rather than the treatment, which was our variable of interest in the analysis. This batch effect was considered in the analysis and the cell line of origin was used as a covariate of the statistical model for the differential expression analysis. A potential outlier sample at the 72-h exposure to A0 (id: Control8_A0) was found and removed from the following analysis steps. Both datasets were balanced by filtering out genes that were not expressed in at least one sample for each group. By using the appropriate function provided by DESeq2 package, differential expression analysis was performed by comparing each exposed group with its relative control group. Benjamini-Hochberg procedure was used for multiple testing correction and only significant genes with an adjusted p-value < 0.05 were kept and used as input for the pathway analysis performed by using QIAGEN IPA software (Krämer et al., 2014; QIAGEN Inc., n.d.).

2.8. TEER measurements

To assess the alterations in epithelial barrier integrity of the OM cultures in ALI after being exposed to the emissions, transepithelial electric resistance (TEER) was used. We utilized a volt/Ohm meter (EVOM2) with STX2 chopstick electrodes (World Precision Instruments) to measure the resistance imposed by the cells at ALI. The EVOM2 was used according to the manufacturer's instructions manual. Before the start of the exposure, the apical OM cells at ALI were washed with D-PBS to remove the mucous followed by measurement of a baseline resistance. Further, the OM cells at ALI were exposed through the apical side to A0, A20, and Euro6 at a concentration of 20 l/ml, for 24-h and 72-h. At the end of the exposure time, the pollutants were removed from the apical side of the tissue culture insert, and both apical and basal chambers were washed with D-PBS before obtaining the endpoint TEER measurement. Each exposure was carried out in triplicates, and both timepoints were performed independently. Actual resistance values were obtained by subtracting the resistance value of the actual exposure from the resistance value obtained from blank inserts. Finally, the TEER values (Ohm/cm^2) were calculated by multiplying the actual resistance with the surface area of the insert. The alteration caused by the emission was represented as a fold change relative to the control.

2.9. Statistical analyses

Statistics were performed with the GraphPad Prism 8.1.0 (GraphPad Software Inc. San Diego, CA, USA) software. The significance of differences between control and experimental values was assessed using the one-way analysis of variance (ANOVA) with Dunnett's post hoc test. Error bars represent the standard deviation (SD). Differences were considered significant at $p \leq 0.05$ if not otherwise stated. For graphical illustrations were utilized features of BioRender.com and the open-source vector graphics editor Inkscape 0.91.

3. Results

3.1. Characterization of A0, A20 and Euro6 samples

Chemical analyses were performed to characterize the contents of metals, polycyclic aromatic hydrocarbons (PAHs), nitrogen compounds (NO_x), organic carbon (OC), and elemental carbon (EC) in the collected UFP samples. In addition, particle size distribution was measured. For A0 and A20 more detailed analysis including OC/EC ratios has been published previously (Hakkarainen et al., 2023), and Euro6-sample characterization is reported elsewhere (Saarikoski et al., unpublished results) The Euro6-sample is very clean, due to the low number of components. Fig. 1a, c, and d thus display results only from A0 and A20 analysis.

3.1.1. Metal contents

Metal concentrations analyzed from PM samples were low, and only a few species exceeded the detection limit of the analysis method (Fig. 1a). Total amount of metals was higher in A20 (10.94 μg/m^3) than in A0 (7.27 μg/m^3). The highest concentrations of metals in A0 were nickel (Ni) and calcium (Ca) while sodium (Na), Ca, and Ni dominated in

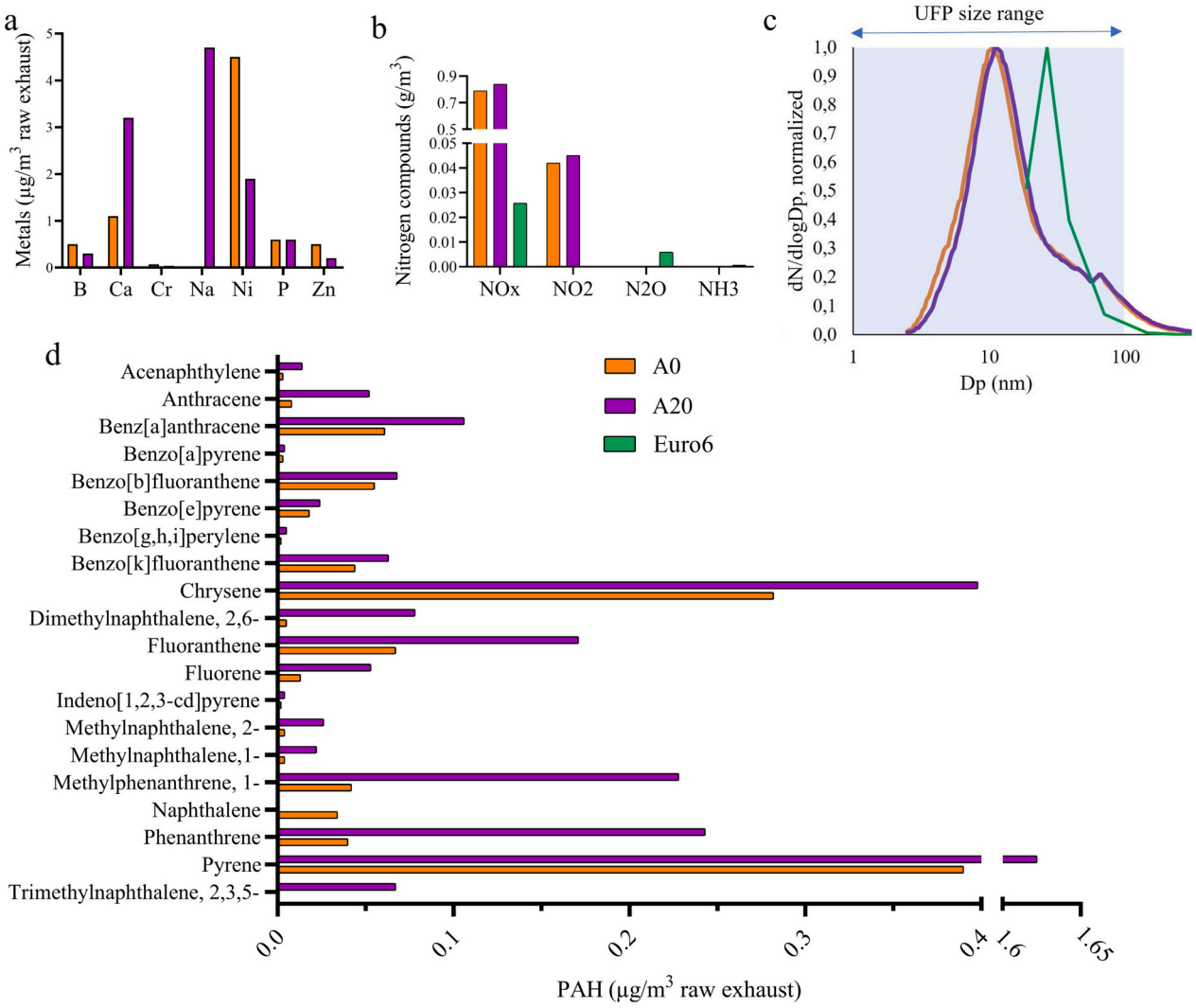

Fig. 1. Characterization data of used samples A0, A20, and Euro6. (a) Metals found in A0 and A20, are presented as a mass of metals per volume of the raw exhaust (µg/m^3). (b) Reactive nitrogen compounds in A0, A20, and Euro6 are presented as a mass of nitrogen compounds per volume of the exhaust (g/m^3). (c) Particle number size distributions for A0, A20, and Euro6 presented as particle diameter (Dp) vs. normalized concentration of particles in the exhaust (dN/dlogDp). (d) Distribution of 20 detected PAHs in A0 and A20, presented as a mass per volume of the raw exhaust (µg/m^3).

A20. Major differences between fuels were observed with Ni (4.5 µg/m^3 [A0] vs. 1.9 µg/m^3 [A20]), Ca (1.1 µg/m^3 [A0] vs. 3.2 µg/m^3 [A20]) and with Na (0 µg/m^3 [A0] vs. 4.7 µg/m^3 [A20]). In addition, small amounts of boron (B), chromium (Cr), phosphorus (P), and zinc (Zn) were also detected in both A0 and A20 (Fig. 1a). However, the majority of the measured metals (Hg, Ag, Al, As, Ba, Be, Br, Cd, Co, Cu, K, Li, Mg, Mn, Mo, Pb, Rb, Sb, Se, Sn, Sr, Th, Tl, U, V) were under the limit of detection. Overall, metal contents seem to be higher in A20 when compared to A0. In the analysis of Euro6 sample, no metals were detected.

3.1.2. *Reactive nitrogen compounds*

Most of the nitrogen exists in the atmosphere as N_2 gas (Nieder and Benbi, 2022). When the bond is broken due to high temperature, N becomes reactive and can form gases such as NH_3 (ammonia), NO_x (nitrogen oxides): NO (nitric oxide), and NO_2 (nitrogen dioxide) and N_2O (nitrous oxide). Measurements of reactive nitrogen compounds (Fig. 1b) resulted in a substantial difference in NO_x levels when comparing A0 and A20 to Euro6. NO_x level for Euro6 was 0.0257 g/m^3, whereas for A0 and A20 the amounts were 0.789 g/m^3 and 0.839 g/m^3, respectively. Roughly stated, NO_x emissions are 30 times higher in A0 and A20 emissions than in Euro6. In addition, NO_2 levels with A0 (0.042 g/m^3) and A20 (0.045 g/m^3) were clearly higher than with Euro6 (0.0002 g/m^3). However, the N_2O level was found to be higher with Euro6 (0.0059 g/m^3), whereas both A0 and A20 had non-detectable amounts. NH_3 level was also observed to be higher with Euro6 (0.0006 g/m^3) when compared to A0 (0.0001 g/m^3) and A20 (0.00001 g/m^3). Overall, these results suggest that amounts of reactive nitrogen products are higher in A0 and A20 compared to Euro6. In addition, A20 seems to produce slightly more NO_x emissions than A0.

3.1.3. *Particle number size distributions*

Fig. 1c shows the normalized exhaust particle number size distributions measured for the samples A0 and A20 from HDE and Euro6 from DI-E6d (Data adapted from Saarikoski et al., unpublished results and Hakkarainen et al., 2023). As the sources and fuel were the same, the particle size distributions represent the collected PM size distribution. Note that, normalized size distributions do not show the particle concentrations, which were significantly smaller in Euro6 than in A0 or A20 samples. In general, the number size distribution data showed that the majority of collected exhaust particles were in particle sizes smaller than 100 nm with all the samples. Thus, the samples used in this study can be considered as UFPs. Importantly, the size distributions of A0 and A20 (from HDE exhaust without exhaust filtration) are typical for that kind of engine, including nanoparticle mode at 10 nm and soot mode in

relatively small particle sizes (Hakkarainen et al., 2023). Also, the particle size distribution of Euro6 from DI-E6d exhaust can be seen as typical particle size distribution for a diesel car with DPF; particles were in low concentrations but in sizes distributions of diesel exhaust soot particles (Saarikoski et al., unpublished results; see also Wihersaari et al., 2020).

3.1.4. Polycyclic aromatic hydrocarbons (PAHs)

A total of 24 PAHs were characterized, out of which 20 PAH compounds were detected. Their mass per cubic meter of the raw exhaust is presented in Fig. 1d. Acenaphthene, biphenyl, dibenz[*a*,*h*]anthracene, and perylene were under the limit of detection. In A0, the major PAHs found were pyrene (0.390 μg/m^3) > chrysene (0.282 μg/m^3) > fluoranthene (0.067 μg/m^3) > benz[*a*]anthracene (0.061 μg/m^3) and >benzo[*b*]fluoranthene (0,055 μg/m^3). In A20, the major PAHs found

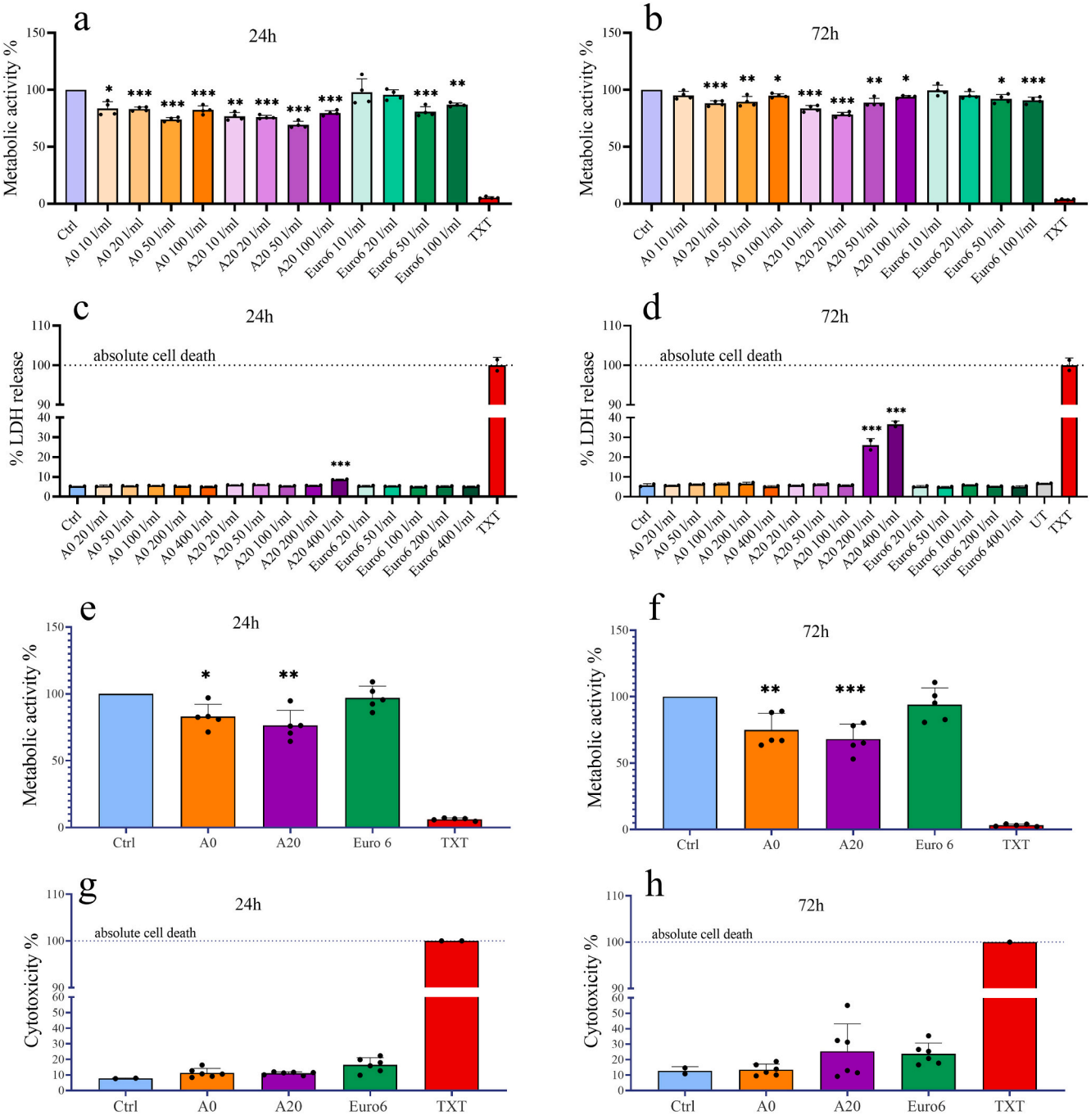

Fig. 2. Assessment of cellular viability. (a, b) MTT reduction assay with multiple concentrations at the 24 h and 72 h exposure. Decrease of metabolic activity compared to the control as assessed with the MTT test after a 24-h and 72-h exposure of OM-cells to different concentrations of UFP samples. All concentrations are compared to their corresponding control. $n = 1$ line, 4 technical replicates. (c, d) LDH release assay with multiple concentrations. Effects of different concentrations of A0, A20, and Euro6 samples on cytotoxicity in OM cultures. Results are shown as a percentage from lysed cell control: TXT (Triton-X treated cells for absolute cell death), n = 1 line, 2 technical replicates. (e, f) MTT with one concentration. OM cells from $n = 5$ individuals upon exposure to different UFPs at a concentration of 20 l/ml. All treatments are compared to the control. (g, h) LDH with one concentration. OM cells from $n = 6$ individuals upon exposure to different UFPs at a concentration of 20 l/ml. Results are shown as a percentage from lysed cell control (TXT). * = $p \leq 0.05$; ** = $p < 0.01$; *** = $p < 0.001$.

were pyrene (1.622 μg/m^3) > chrysene (0.398 μg/m^3) > phenanthrene (0.243 μg/m^3) > 1- methylphenanthrene, (0.228 μg/m^3) > fluoranthene (0.171 μg/m^3).

The dominant PAHs were: 3- (phenanthrene, 1- methylphenanthrene) 4- (pyrene, chrysene, fluoranthene, benz[*a*]anthracene), and 5-ring (benzo[*b*]fluoranthene) PAHs, most of them classified as carcinogenic and mutagenic substances (Kim et al., 2013). All measured PAHs were found to be higher in A20 than in A0, except for naphthalene. This 2-ring PAH was not detected in A20 while in A0 it was the ninth highest (0.034 μg/m^3) PAH. However, in A20, dimethylnaphthalene, 2.6- and trimethylnaphthalene, 2.3.5- were found among the top 10 measured PAHs. Overall, the differences in PAH compositions between A0 and A20 were substantial and indicate the large difference between distillate and hydrotreated fuel.

3.2. Effects of emissions on cytotoxicity and cellular metabolism in OM cells

Firstly, we defined the lowest effective dose at which a response occurs in OM cells. Cellular metabolism was measured with the MTT reduction assay following exposure to exhaust UFPs for 24-h and 72-h (Fig. 2a and b). OM cells derived from one individual were treated with different concentrations (10, 20, 50, and 100 l/ml) of A0, A20, Euro6 samples. Timepoints were selected to represent more acute response (24-h) and slightly prolonged exposure (72-h) to see whether response differs upon different durations.

At the 24-h timepoint, exposures to A0 and A20 showed a slight but statistically significant reduction in metabolic activity with a concentration of 10 l/ml when compared to the control (Fig. 2a). However, exposure to Euro6 caused a significant reduction in cellular metabolism only at the higher concentration of 50 l/ml. At the 72-h timepoint (Fig. 2b), exposure to A0 resulted in a significant decrease of metabolic activity with concentrations of ≥20 l/ml, whereas exposure to A20 elicited a significant reduction with all the tested concentrations. Exposure to Euro6 reduced metabolic activity with higher concentrations of 50 l/ml and 100 l/ml. This suggests that with exposures to A0 and A20 significant decrease in metabolic activity was reached with relatively low concentrations, whereas the Euro6 sample required a 2.5–5 times stronger dosage to cause a significant decrease in MTT assay. When comparing the two time points, 24-h and 72-h, it seems that cells elicit a stronger response to UFPs with the shorter exposure time (24-h), especially with higher concentrations of 50 l/ml and 100 l/ml. This might be explained by an acute reaction, which plateaus to some extent with increasing time, although the magnitude of the differences overall were relatively modest.

To see whether any of these concentrations cause cell death, cellular toxicity upon 24-h and 72-h UFP treatment was assessed by the lactate dehydrogenase (LDH) release assay in one representative OM cell line exposed to various concentrations (20, 50, 100, 200, and 400 l/ml) of A0, A20, and Euro6 (Fig. 2c and d). Lysed cells (Triton-X treated) serve as an indicator for absolute cell death (100 %). No cytotoxicity was observed in response to A0 and Euro6 exposure in any of the tested concentrations when compared to the control at either timepoint. However, at the 24-h timepoint cells exposed to A20 with the highest concentration of 400 l/ml (Fig. 2c) showed a slight but statistically significant increase in cytotoxicity. Whereas, at the 72-h timepoint exposure to A20 with a concentration of 200 l/ml already displayed significant toxicity in addition to a concentration of 400 l/ml (Fig. 2d). This suggests that only exposure to A20 manifests signs of toxicity with substantially high concentrations, and longer exposure time increase the cytotoxicity. Even though UFPs may not cause significant cell death until with substantially high concentrations as assessed by LDH release (Fig. 2c and d), they can still have detrimental effects on cell functions even with lower doses, as shown by results of the MTT assay (Fig. 2a and b). Due to the limited number of the samples (especially of A0 and A20), it was essential to determine the lowest effective dose at which a response occurs. Thus, based on the resources and these findings we decided to continue further experiments with the UFP concentration of 20 l/ml and both time points of 24-h and 72-h. Using the same dose and timepoint for all emissions will allow us to decipher whether there exist differential responses of the OM cells to these fuels. To analyze further the selected concentration of 20 l/ml, and specifically the donor-to-donor variation in cellular responses, we exposed OM cells from different individuals (n = 5) to A0, A20, and Euro6 samples and performed the MTT viability assay (Fig. 2e and f). At the 24-h and 72-h timepoints we observed a statistically significant decrease in metabolic activity compared to the DMSO control with exposures to A0 and A20. However, exposure to Euro6 did not affect cellular metabolic activity compared to the control. Response to A20 was stronger in both timepoints compared to A0 and Euro6. We also noted the donor-to-donor variation inside treatments, and it seemed to be enlarged with longer exposure. These trends suggest that despite the variation between donors, the most severe decrease in viability appears to be with exposure to A20 in both timepoints. Cellular toxicity upon 24-h and 72-h pollutant treatment was again assessed by LDH assay. The LDH assay was performed on OM cells from different individuals (n = 6) exposed to the 20 l/ml concentration of A0, A20, and Euro6 (Fig. 2g and h). No significant cytotoxicity was observed in response to any of the exposures when compared to control in either timepoint. It is however notable that at the 72-h timepoint with exposure to A20, the deviation is large. This suggests that 72-h exposure to A20 is causing eminently diverse responses between OM cells from different individuals.

3.3. Transcriptomic analysis revealed substantial numbers of differentially expressed genes (DEGs) with exposures to A0 and A20

Having confirmed suitable effective concentration to expose OM cells without causing cell death, to gain insight into molecular level mechanisms in OM upon exposure, we performed total RNA-Seq on UFP-treated OM cells derived from different individuals (n = 6) in two different timepoints.

At the 24-h timepoint differential expression analysis resulted in 1690 DEGs in A0 exposed cells with respect to control cells (812 upregulated and 878 downregulated) (Fig. 3a; See Supplementary Table S1 for a full listing of all DEGs), while exposure to A20 resulted in 1912 DEGs (892 upregulated and 1020 downregulated) (Fig. 3b; Table S1). However, only 9 genes were differentially expressed upon 24-h exposure to Euro6 compared to control cells (6 upregulated and 3 downregulated) (Fig. 3c; Table S1). DEGs having an adjusted p-value lower than 0.05 were included in the analysis. The overlap of differentially expressed genes in Fig. 3g shows that the majority of DEGs are shared between A0 and A20, although both still have a substantial portion of exposure-specific genes. In addition, Euro6 exposure seems to elicit similar effects as exposures to A0 and A20, although the magnitude of the responses is considerably smaller.

At the 72-h timepoint differential expression analysis revealed 866 DEGs upon exposure to A0 with respect to control cells (376 upregulated and 490 downregulated) (Fig. 3d; Table S1), and exposure to A20 resulted in 3719 DEGs (1681 upregulated and 2038 downregulated) (Fig. 3e; Table S1). Again, only 13 genes were found to be differentially expressed upon 72-h exposure to Euro6 when compared to control cells (1 upregulated and 12 downregulated) (Fig. 3f; Table S1). Overlap of differentially expressed genes at the 72-h timepoint in Fig. 3h revealed that the majority of DEGs found upon exposure to A0 are shared with A20. However, the total amount of genes found solely in exposure to A20 is remarkable. Again, the effect of Euro6 exposure seems to be incremental, having only a few shared genes in comparison to A0 and A20.

Notably, the most prominent transcriptional changes with respect to the number of DEGs were observed with the 72-h exposure to A20, while exposure to Euro6 seems to cause only minor alterations compared to A0 and A20 exposures. Overall, these findings suggest that A20 has the most significant impact on OM cells' altered gene expression. Furthermore,

Fig. 3. Transcriptomic alterations caused by exposures to A0, A20, and Euro6 at timepoints of 24-h and 72-h. (a, b, c) Heatmaps showing the scaled expression of differentially expressed genes (p-adjusted < 0.05) upon a 24-h exposure to A0, A20, and Euro6. (d, e, f) Heatmaps showing the scaled expression of differentially expressed genes (p-adjusted < 0.05) upon a 72-h exposure to A0, A20, and Euro6. In all the heatmaps, the top 15 most down- and upregulated genes are shown for A0 and A20 while for Euro6 all the differentially expressed ones are presented. (g, h) Venn diagrams showing the number of shared differentially expressed genes between A0, A20, and Euro6 exposures at different timepoints (24-h and 72-h).

the longer exposure seems to elicit a stronger impact than the shorter more acute exposure time. However, exposure to A0 caused a stronger response with shorter 24-h exposure than with 72-h exposure. Given the vast amount of DEGs found, we decided to focus mainly on the top 15 up and downregulated genes based on the log2FC-value within each treatment per timepoint to understand the major manifestations behind altered gene expression in OM-cells upon the UFP exposure. We aimed to explore if there is a common nominator for the bigger subset of genes and if we can find correlations to prior literature. We were not interested in one specific gene which was highly differentially expressed, but more like a set of genes telling the same story.

3.3.1. Transcriptomic alterations related to inflammation and xenobiotic metabolism

As previously reported by others, PM exposure can cause diverse reactions in cells varying from oxidative stress and inflammation to cell death. In our data, the most upregulated gene found at the 24-h timepoint in exposures to A0 (Fig. 3a *log2FC 3.86*) and A20 (Fig. 3 b *log2FC 3.78*) was *GPR68*, which is a mediator of respiratory inflammatory responses (Huang et al., 2015). In addition, *CD7*, associated with inflammation in nasal mucosa (Morinaka and Nakamura, 2000) was found to be highly upregulated at both timepoints of 24-h (Fig. 3a; *log2FC 2.84* [A0] and Fig. 3b; *log2FC 2.98* [A20]) and 72-h (Fig. 3d; *log2FC 2.95* [A0] and Fig. 3e; *log2FC 3.70* [A20]). Contrary to previous reports of upregulation during inflammatory processes, *A2M* in the nasal mucus (Tomazic et al., 2014) and *IL32* in vascular endothelial cells (Nold-Petry et al., 2009), these two genes were highly downregulated at 72-h exposure to A0 (Fig. 3d; *log2FC −2,04*) and to A20 (Fig. 3e; *log2FC −3.38*), respectively.

Interestingly, *CYP1A1*, known to metabolize PAHs (Kang et al., 2020), was upregulated at the 24-h timepoint with exposures to all the tested samples, A0 (*log2FC 2.47*), A20 (*log2FC 2.70*) and Euro6 (*log2FC 2.05*) (Fig. 3a, b, c respectively). However, at the 72-h timepoint, only exposure to A0 (Fig. 3d) and A20 (Fig. 3e) resulted in upregulation of *CYP1B1* (*log2FC 2.87* [A0] and *log2FC 3.22* [A20]). Furthermore, at the 24-h timepoint among the top 15 most downregulated genes with exposures to A0 and A20 (Fig. 3a and b) were found the genes *INMT (log2FC −3.04* [A0], *−3.54* [A20]*), FMO1* (*log2FC −2.48* [A0], *−2.68* [A20]) (Watson et al., 2013) *GSTA1* (*log2FC −1.62* [A0], *−2.48* [A20]) (Schwartz et al., 2020) associated with xenobiotic metabolism. At the 72-h exposure to A0, (Fig. 3d) *FMO1* (*log2FC −2.24*), as well as FMO2 (log2FC −2.01), were found in the top 15 most downregulated genes. In exposure to Euro6 at the 24-h timepoint (Fig. 3c) was found the gene *SECTM1* (*log2FC 1.21*), which has been previously reported to be upregulated upon exposure to PAH benzo(*a*)pyrene (Kaarthik et al., 2009). This gene was also up-regulated with the 72-h exposure to A20 (*log2FC 2.62*) (Fig. 3e). Lastly, at the 72-h timepoint the most upregulated gene found in exposures to A0 (Fig. 3d; *log2FC 3.51*) and A20 (Fig. 3; *log2FC 4.88*) was *NPTX1*, which has previously shown by our research group to be upregulated upon exposure to urban PM in OM cultures (Chew et al., 2020). This gene was also up-regulated with the 24-h exposure to Euro6 (Fig. 3c). Taken together, our findings from the differential expression analysis are in line with the current literature concerning inflammatory responses and xenobiotic metabolism and provide new insight into the effects of UFPs in cultures of OM cells.

3.3.2. Transcriptomic alterations in olfactory signaling

Considering the specialized role of the OM in odor perception, we were exceptionally interested to discover UFP-induced alterations in genes associated with olfactory signaling. For example, *GAD1* (Glutamate Decarboxylase 1) was among the top 15 upregulated genes at the 24-h exposure to A0 (Fig. 3a; *log2FC 2.19*) and within the top 40 genes altered upon exposure to A20 (Fig. 3b; *log2FC 2.09*). In addition, genes associated with olfactory functions, *LEP* (Sun et al., 2019) and *GSTA1* (Schwartz et al., 2020), were found downregulated at the 24-h exposures to A0 (*log2FC −2.50* and *−1.62* respectively) and A20 (*log2FC −2.87* and *−2.48* respectively). In addition, *TAS2R* belonging to the chemosensory receptors (di Pizio et al., 2019), was downregulated with A0 (*log2FC −2.49*) and A20 (*log2FC −2.56*) exposures. At the 72-h timepoint the most downregulated gene in exposure to A20 (Fig. 3e; *log2FC −4.14*) and fifth most downregulated in exposure to A0 (Fig. 3d; *log2FC −2.59*) was *KISS1*, an important neuropeptide which has been visualized in olfactory bulb (OB) and its role in mediating signals through olfactory route to the brain has been established with both animal and human studies (Mills et al., 2022). Interestingly, also *LEP* was among the most downregulated genes at the time point of 72-h with A0 (Fig. 3d; *log2FC −2.48*) and A20 (Fig. 3e; *log2FC −3.38*) exposures. In addition, at the 72-h exposure to A20 (Fig. 3e), we discovered several upregulated genes further supporting findings of altered olfactory signaling, such as *PYY2* (*log2FC 2.52*), a rather poorly known pseudogene and member of the neuropeptide family (Couzens et al., 2000). This gene has been previously reported to have an important role in the regulation of olfactory neuron differentiation in mouse olfactory neuroepithelium (Doyle et al., 2012). In addition, among the top 15 DEGs upon 72-h exposure to A20, we found *PTPRN* (*log2FC 2.51*) previously reported as an activity-dependent gene in mouse olfactory sensory neurons (Fischl et al., 2014) and *GABRA3* (*log2FC 2.56*), the receptor of inhibitory neurotransmitter GABA (Agapite et al., 2022). Taken together, these results suggest that exposure to A0 and A20 causes altered expression of genes related to olfactory signaling in human primary OM cell cultures.

3.3.3. Transcriptomic alterations related to compromised epithelial barrier functions

Based on the existing knowledge of PM's ability to hamper epithelial functions in other tissues, we were interested to see whether these changes also manifest in human primary OM cells. Keratins are important components of the cytoskeletal network providing support for cells but also building connections between adjacent cells and extracellular matrix (ECM), therefore playing an important role in regulating the integrity of epithelial tissues (Yu et al., 2022). At the 24-h timepoint in exposure to A0 (Fig. 3a) and A20 (Fig. 3b), among the most downregulated genes was *FLG* (*log2FC −2.87* [A0], *−2.71* [A20]), which is known to be involved in the maintenance of the epidermal barrier by aggregating keratin filaments to form a keratin network (Kim and Lim, 2021; Nakamura et al., 2021). Furthermore, 72-h exposure to A20 (Fig. 3e) revealed several keratins among the top 15 downregulated genes: *KRT81* (*log2FC −3.56*), *KRT7* (*log2FC −3.44*), *KRT86* (*log2FC −3.36*) and *KRT80* (*log2FC −3.08*), as well as *PADI1* (*log2FC −3.20*), which is known to be involved in filaggrin and keratin processing (Merleev et al., 2022). In addition, *TRPA1*, reported to regulate keratinocyte differentiation and mediate inflammatory skin responses (Atoyan et al., 2009), was highly upregulated at the 24-h exposure to A20 (*log2FC 2.72*). However, exposure to A0 at the 72-h timepoint resulted in only one downregulated keratin, *KRT86* (*log2FC −2.06*). Genes known to be key players in the formation of tight junctions (TJ) (Zihni et al., 2016), *CLDN1* (*log2FC −2.35*), *OCLN* (*log2FC −1.25*), and *MAGI1* (*log2FC −0.40*), were also found to be downregulated at the 72-h exposure to A20 (Table S1). Considering the pivotal role of proper ECM stiffness in maintaining epithelial barrier permeability (Mammoto et al., 2013), it was interesting to find the main fibrous ECM proteins, collagens and elastin (Liu et al., 2021), to be well represented among all DEGs. One of the most upregulated genes in exposure to A20 at the 24-h timepoint was *COL28A1* (Fig. 3b; log*2FC 3.00*) and at the 72-h timepoint *COL26A1* (Fig. 3e; *log2FC 2.64*). At the 72-h exposure to A20, among all DEGs (Table S1) we found 14 additional members of the collagen family. Whereas exposure to A0 at the 72-h timepoint resulted only in one DEG *COL5A3* (Table S1; *log2FC 1.02*). However, *ELN* was downregulated in exposures to A0 and A20 at both timepoints of 24 h (*log2FC −2.00* [A0] and *−2.20* [A20]) and 72-h (*log2FC −1.83* [A0] and *−2.59* [A20]) (Table S1). Taken together, these results suggest that several genes coding vital components in epithelial integrity maintenance are

downregulated in OM cells upon exposure to A0 and A20, with A20 causing a more severe impact.

3.4. Pathway analysis

Since differential expression analysis resulted in a vast amount of DEGs, we harnessed Ingenuity Pathway Analysis (IPA) features to suggest the cellular pathways affected by exposure to different emissions. IPA predicted several cellular pathways to be inhibited and a few being activated upon exposures to A0 and A20 in both timepoints. The most significant pathways of our interests in both timepoints are presented in Fig. 4a and b. Only pathways with z-scores ≥ 2 or ≤ -2 and $-\log(p\text{-value}) \geq 1.3$ were considered significant (see Supplementary Data Table S2 for a full listing of pathways and genes for each pathway). Euro6 exposure did not elicit any significant pathways in either timepoint, therefore not included in the figures.

At the 24-h timepoint (Fig. 4a), the exposure to A0 resulted in 28 inhibited and 3 activated pathways. Exposure to A20 caused the inhibition of 99 pathways, while 3 were upregulated. One of the most significant pathways observed with both exposures to A0 and A20 was EIF2 Signaling, with z-scores of −3.272 and −2.785 respectively. Other common significant pathways observed with both exposures to A0 and A20 were Integrin Signaling (z-scores −2.744 [A0] and −3.592[A20]), ILK Signaling (z-scores −2.646 [A0] and −3.536 [A20]), Actin Cytoskeleton Signaling (z-scores −3,024 [A0] and −3.286 [A20]), Signaling by Rho Family GTPases (z-scores −2.921[A0] and −3.43 [A20]) and Regulation of Actin-based Motility by Rho (z-scores −2.357[A0] and −2.524 [A20]). Among the few activated pathways, we found RHOGDI-Signaling, which was significant in both exposures (z-scores 3 [A0] and 3.138 [A20]) and PPAR signaling (z-score 2.496) which was significant only with exposure to A20. Although there were many common pathways observed, there were still some unique pathways with both exposures. In exposure to A0, the most significant unique pathways were inhibited Oxidative Phosphorylation (z-score = −4.123) and activated Granzyme A Signaling (z-score = 2.111). With exposure to A20, major differences found in comparison to A0 were Pulmonary Fibrosis Idiopathic Signaling Pathway (z-score −3.13), VEGF Signaling (z-score −2.982), IL-8 Signaling (z-score −2.556), Acute Myeloid Leukemia Signaling (z-score −3.153), Regulation Of The Epithelial Mesenchymal Transition By Growth Factors Pathway (z-score −3.536), IL-3 Signaling (z-score −2.668), Thrombopoietin Signaling (z-score −2.324) and Insulin Receptor Signaling (z-score −2.711).

The 72-h exposure (Fig. 4b) to A0 resulted in 4 inhibited pathways, while exposure to A20 revealed 72 inhibited and 8 activated pathways. All pathways found with exposure to A0 were also observed with exposure to A20. These pathways and their z-scores were Actin Cytoskeleton Signaling (z-scores) (z-score = −2.236 [A0] and z-score = −4.811[A20]), Integrin Signaling (z-score = −2.5 [A0] and z-score = −3.873[A20]), ILK Signaling (z-score = −2.138 [A0] and z-score = −2.1 [A20]) and Paxillin Signaling (z-score = −2.121 [A0] and z-score = −3.4 [A20]). In addition, at the 72-h exposure to A20, other significant pathways were Signaling by Rho Family GTPases (z-score = −3.457), RHOA Signaling (z-score = −2.846), Regulation of Actin-based Motility by Rho (z-score = −2.694), RAC Signaling (z-score = −4), Pulmonary Fibrosis Idiopathic Signaling Pathway (z-score = −2.619), Actin Nucleation by ARP-WASP Complex (z-score = −3), Ephrin Receptor Signaling (z-score = −3.317), Remodeling of Epithelial Adherens Junctions (−log(p) = 5.77, z-score = −2.121), Wound Healing Signaling Pathway (z-score = −3.414) and PI3K/AKT Signaling (z-score = −4.7). The activated pathways found in exposure to A20 were RHOGDI-Signaling (z-score = 3.13), PTEN signaling (z-score = −3.182), Sonic hedgehog signaling (z-score = 2.111), and PPAR signaling (z-score = 2.524). Overall, the most prominent impact on biological processes concerning the altered pathways seems to be with exposure to A20.

3.5. Permeability measurements validate transcriptomic changes

Since one of the most prominent alterations observed in transcriptomic analyses was related to membrane permeability upon UFP exposure, we next validated our findings of the compromised epithelial barrier function of the OM using transepithelial electric resistance measurements. For this purpose, we cultured the OM cells in ALI, exposed them to UFPs with a concentration of 20 l/ml, and performed TEER-measurements (Fig. 5a) at 24-h and 72-h timepoints. In the 24-h timepoint, (Fig. 5b) exposure to A20 UFP shows a statistically significant decrease in relative TEER compared to the control. A0 or Euro6 exposure did not affect the TEER values. In the 72-h timepoint (Fig. 5c), exposure to both A0 and A20 resulted in a significant reduction in relative TEER when compared to the control. Euro6 UFP shows a slight but statistically significant decrease in the TEER with longer 72-h exposure. We have compared the originally measured TEER values to the corresponding expression level of genes involved in epithelial barrier functions within the same cell line ($n = 1$) upon each UFP exposure (Supplementary Fig. 1). The scatterplots (Fig. S1) present the correlation of DEGs mentioned in the results section 3.3.3 and in addition, some genes from Actin Cytoskeleton Signaling, Signaling by Rho Family GTPases, and Integrin Signaling pathways. From the scatterplots (Fig. S1) we can observe, depending on the log2FC-value of the genes, that for the majority of the listed genes, a lower TEER value corresponds with lower gene expression or vice versa. These findings suggest that exposure to UFPs can affect the epithelial barrier function in OM cells with some time-dependent effects and that exposure to A20 UFP seems to elicit the strongest effect on membrane permeability.

4. Discussion

The aim of this study was to provide new insight into the impacts of exhaust emissions on the human olfactory mucosa by comparing the exposure effects of different fuels and engine technologies. Given the lack of knowledge in this area, we were especially interested in the effects of the UFP fraction of the emissions.

We first characterized the emissions by analysis of chemical composition and size. Analysis of metal content revealed that only low amounts of metals were found in A0 and A20 samples. Most of the analyzed metals were below detection limits and even those that were detected might be residues of lubricant oils or engine wear (Rönkkö and Timonen, 2019). In A0 the most abundant metal found was nickel (4.5 $\mu g/m^3$). According to WHO air quality guidelines for Europe, the incremental risk level for nickel in the air is 1 $\mu g/m^3$ (World Health Organization. Regional Office for Europe., 2000). Occupational nickel exposure has been connected to olfactory impairment and toxicity in the olfactory tract has been shown also in rodents (Sunderman, 2001). The A20 sample consisted mostly of sodium and calcium comprising roughly 72 % of the total metals found in the sample. Similar results have been reported earlier with Euro3 vehicles, stating that these metals are components of lubricant oils (Alves et al., 2015). Total NO_x emissions and NO_2-levels alone were found to be extremely high with A0 and A20, which was expected since the HDE did not contain any aftertreatment device to reduce NO_x emissions. The recommended NO_2-level by WHO air quality guidelines is 10 $\mu g/m^3$ Since the 1990s due to the regulation of emissions, NO_x concentrations have been decreasing in Europe and USA but instead, in the developing world they are still increasing (Nieder and Benbi, 2022). In our opinion, it is possible that this amount of NO_x released in the air could cause adverse health effects and alter the functions of OM cells.

Size distribution analyses revealed that all the samples in this study consist mainly of UFPs, with HDE samples A0 and A20 having higher concentrations of the smallest particles, compared to the Euro6 sample. According to the prior literature, the smallest particles may cross membranes most easily (Kwon et al., 2020), and possibly reach the brain (Schraufnagel, 2020) suggesting that A0 and A20 might be more

Fig. 4. The cellular pathways affected by the exposure to A0 and A20. (a) Barplot showing the level of significance and the enrichment score of the 20 most interesting pathways provided by IPA, analyzing A0 and A20 differentially expressed genes after the exposure for 24-h, (b) and 30 most interesting pathways provided by IPA, analyzing A0 and A20 differentially expressed genes after the exposure for 72-h.

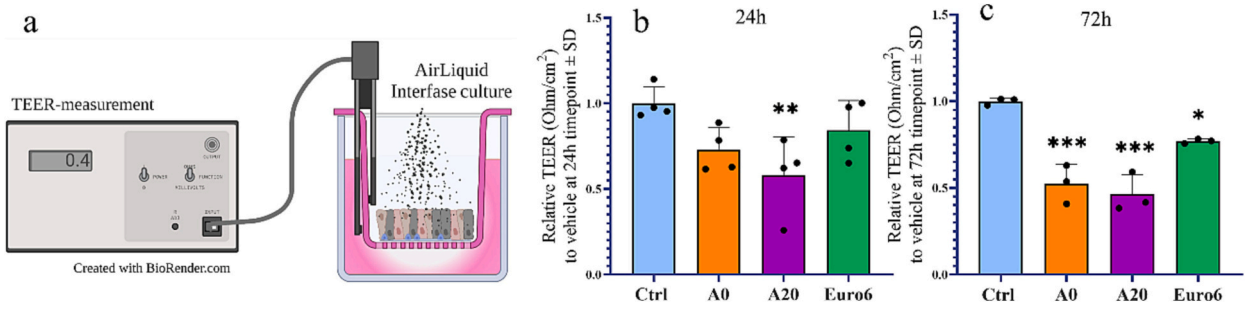

Fig. 5. Transepithelial electric resistance (TEER) (a). Illustration of the experimental setup. (b) Decrease of epithelial barrier integrity compared to control as assessed with the TEER-measurement after 24-h and (c) 72-h exposure to different UFPs at a concentration of 20 l/ml. Results are shown as a relative change to control. Asterisks indicate a statistically significant difference in exposure from the control. n = 1 primary OM cell line, 3-4 technical replicates. * = $p \leq 0.05$; ** = $p < 0.01$; *** = $p < 0.001$.

harmful to the functions of OM cells. PAH contents revealed A20 containing substantially larger amounts of different PAHs, demonstrating the difference between fossil and renewable diesel. Overall, PAH contents were similar to those previously reported in diesel vehicle exhaust (Zhang et al., 2019), having pyrene, chrysene, phenanthrene, and fluoranthene as dominating species. Furthermore, these PAHs are typically bound to particles with a diameter of <1 μm and therefore able to travel long distances in the atmosphere and enter the bloodstream reaching multiple organs including the central nervous system (Zhang et al., 2019). The most notable difference in PAH contents between fuels was observed with the levels of phenanthrene and 1- methylphenanthrene, which both were found clearly higher in A20 compared to A0 and previously have been shown to cause toxicity (He et al., 2022; Le Bihanic et al., 2014). In this study viability assays showed that exposure to A0 and A20 samples reduced the metabolic activity of the OM cells without causing significant cytotoxicity. Cytotoxicity, assessed by the LDH-release assay, was reached upon using high exposure concentrations of 200 l/ml and 400 l/ml and even then, observed only with the A20 sample. The higher cytotoxicity of A20 compared to A0 might be partially explained by the higher level of phenanthrene and 1-methylphenanthrene.

Chemical characterization of the Euro6 sample confirmed it to be very clean, as only some nitrogen-related compounds were identified, and these were low in comparison to the levels observed in the A0 and A20 samples. The comparison of the A0 and Euro6 samples, which both contained the same fuel but different engines, clearly demonstrated the effectiveness of selective catalytic reduction (SCR) technology in cutting down total NO_x emissions in the Euro 6d-temp engine. In addition, based on the particle size distribution, it seems the Euro6 sample is composed of slightly larger average PM size fractions, which may partially explain less harmful effects. PAH contents of Euro6 were not measured due to the challenges of analyzing these low amounts of PAHs. Overall, the differences between the Euro6-sample and A0 & A20- samples were expected since DI-E6d was equipped with DPF and SCR, whereas HDE did not have any exhaust aftertreatment devices.

Taken together, it can be concluded that exhaust aftertreatment systems have a major impact on the levels of harmful substances found in diesel vehicle emissions. Notable also is the difference observed between fossil and renewable diesel. Renewable diesel seems to be slightly less harmful on a cellular level in OM than fossil diesel. A0 and A20 samples contain relatively large amounts of nitrogen compounds, they mainly consist of UFPs and contain a wide repertoire of different PAHs. Based on the previous studies we suspect these factors to be the main mediators of cellular disruption and the harmfulness of A0 and A20 may indeed lie in the synergism of UFPs and their bound compounds, such as PAHs (He et al., 2022; Kwon et al., 2020; Le Bihanic et al., 2014; Schraufnagel, 2020; Zhang et al., 2019).

On the gene expression level, the same trend with different samples was observed. Exposure to A20 elicited the strongest response in both timepoints, while Euro6 caused only minor changes on the transcriptomic level. However, it was interesting that A0 caused a relatively strong effect on gene expression with a shorter exposure time of 24-h, but not with a longer exposure time of 72-h. A similar effect was seen in MTT at the 24-h exposure where a significant reduction in viability was seen with several concentrations but at the 72-h timepoint, responses were slightly weaker. This might be explained by an acute reaction, which plateaus with increasing exposure time. It is also possible that something in the chemical composition of A0 changes over time, which changes the response. By focusing on the top 15 DEGs in each exposure, we observed that the same types of genes appeared similarly with all of the exposures and in both timepoints, and furthermore, they were supported by the Ingenuity Pathway Analysis-features. Another reason for the single-gene-level examination was to find links between single compounds found in the emission characterization-data. To our knowledge, this kind of linking has not been performed earlier, so therefore this approach was selected. One of the most common cellular responses related to air pollution exposure is inflammation, as shown in several animal models, for example via NLRP3 inflammasome pathway (Jia et al., 2021; Li et al., 2021; Ogino et al., 2014), in vitro models (Mazzarella et al., 2007; Zarcone et al., 2016) as well as in epidemiological studies (Zhang et al., 2022). Furthermore, this has also been seen in the epidemiology of UFP (Clifford et al., 2018). However, to this date, the exact mechanisms of exposure-induced inflammation in the human OM have not been clearly demonstrated. A review by Imamura and Hasegawa-Ishii concluded that infiltration of immune cells and production of inflammatory cytokines are the major initiators of inflammatory response upon exposure to environmental toxicants in the OM (Imamura and Hasegawa-Ishii, 2016). In addition, our previous study demonstrated elevated cytokines upon exposure of OM cells to urban PM (Chew et al., 2020). In the current study, transcriptomic analyses revealed that the most prominent gene upregulated after both 24-h and 72-h exposures to A0 and A20 was *CD7*, an immunoglobulin associated with inflammation in the nasal mucosa (Morinaka and Nakamura, 2000). However, we also observed the downregulation of certain inflammatory genes, such as *A2M* and *IL32*, and in IPA analyses IL-8 Signaling was among the most inhibited pathways. It has been previously reported that PAHs might modulate immunity and disrupt endocrine systems (Vogel et al., 2020; Zhang et al., 2016). In addition, the activation of Peroxisome proliferator-activated receptor α (PPARα) might regulate the inflammatory process by suppressing the release of cytokines and chemokines, for instance via blocking NLRP3 inflammasome activation (Grabacka et al., 2021). In our data, PPAR signaling was one of the few upregulated pathways observed in exposure to A20 at both timepoints. PPARγ activity has previously been shown to be increased with exposure to diesel particulate matter, possibly through the binding of benzo[*e*]pyrene, benzo[*a*]pyrene, and other related chemicals to the receptor (Jeong et al., 2021). Regulation of PPARγ stability is mediated by the aryl hydrocarbon receptor (AHR), to which

PAHs are known to bind and activate the receptor (Vogel et al., 2020). Taken together, it is plausible that PAHs present in A0 and A20 cause AHR-mediated upregulation of PPAR Signaling in the OM cells, causing suppression of the release of cytokines observed in the sequencing data.

AHR also regulates the expression of genes for xenobiotic metabolizing enzymes, such as cytochrome P450 (CYP) (Vogel et al., 2020). Several CYPs were upregulated upon exposure to all emissions, with A0 and A20 eliciting a stronger response than Euro6. The strongest effect was observed with A20 which correlates with the highest PAH-contents of the sample. Activation of *CYP1A1* upon exposure to exhaust emissions has been reported in lung cells (Sima et al., 2022) and upon exposure to urban PM in OM cells (Chew et al., 2020). In addition, PM_{10} exposure upregulates both *CYP1A1* and *CYP1B1* in lung epithelial cells (Kang et al., 2020). Interestingly, the supportive sustentacular cells of the olfactory epithelium are known (among their many other functions) to express xenobiotic metabolizing CYPs in the mouse and human OM (Sammeta and McClintock, 2010; Schwartz et al., 2020). Thus, in line with the literature, our results demonstrate that exposure to UFPs induces CYP-enzymes in OM cultures. However, other genes associated with xenobiotic metabolism, such as *FMO1* and *FMO2*, were downregulated upon exposure. This was unexpected, given that nitrogen compounds, substrates of FMO, were abundant in the A0 and A20 samples. A connection between excessive nitric oxide and olfactory dysfunction has been shown with silkworms exposed to organophosphate (Chen et al., 2022), and the association between NO_2 and olfactory dysfunction in older adults has also been reported (Adams et al., 2016). Considering the high NO_x contents of A0 and A20, these results suggest that FMO-mediated N-oxygenation is somehow suppressed in OM cells upon exposure and it may affect olfactory function. One study demonstrated that AHR-mediated toxicity caused by its known agonist TCDD, suppressed *FMO1* and *INMT* expression while increasing *CYP1A1* and *CYP1B1* in rat liver (Watson et al., 2013). On the contrary, *FMO2* was found to be upregulated in bronchial epithelial cells upon exposure to extractable organic matter from PM, collected from gasoline emissions (Sima et al., 2022). Overall, the roles of *FMO*s and *INMT* in air pollution exposure studies are not well understood and require further research. High amounts of PAH observed in A0 and A20 samples may indicate that alterations in inflammatory cascade and xenobiotic metabolism upon exposure are mediated by AHR in OM, with PAHs being the main culprit. Since the number of human studies investigating this is low (Chang et al., 2019; Wang et al., 2017a), future studies could be targeted at AHR-related mechanisms for increased understanding.

Enzymes such as CYPs and glutathione transferases (GSTs) are known to metabolize and presumably clear odorant chemicals from the olfactory system to prevent their accumulation and thereby keeping chemical stress within the epithelium at low to moderate levels (Sammeta and McClintock, 2010; Schwartz et al., 2020). We found *GSTA1* to be among the most downregulated genes at the 24-h exposure to A0 and A20, which might indicate the impaired capability to clear odors and deal with cellular stress. GSTA1 and GSTP, both members of the GST family, have been previously identified in human nasal mucus and human olfactory sustentacular cells (Durante et al., 2020), and reduced expression of GSTP has been connected to impaired olfactory sensitivity among the elderly (Schwartz et al., 2020). Our results could thereby indicate that the fine-tuning of odors is disrupted in the OM upon exposure to UFPs, thereby negatively affecting odor perception capability. It is suggested that odorant metabolizing enzymes in the olfactory system might be affected by environmental pollutants causing oxidative stress leading to disrupted olfactory perception (Wei et al., 2021). In support of this, earlier reports have suggested a link between high air pollution levels and olfactory function (Adams et al., 2016; Ajmani et al., 2016; Genter and Doty, 2019; Werner and Nies, 2018).

While we did not observe olfactory receptor alterations upon exposure, we found several genes that have previously been associated with olfactory signaling. Kisspeptin1 (KISS1) is a neuropeptide known to mediate signals from the OB to deep brain areas (Mills et al., 2022). Although KISS1-neurons have been identified to be expressed in fetal OM (Morelli et al., 2008) to date, no connection between KISS1, OM, and air pollution exposure has been demonstrated. Here we showed that the gene coding KISS1 was highly downregulated after 72-h exposure to A0 and A20. The observed downregulation allows us to speculate whether the dysfunction of this neuropeptide could result in impaired signaling from the OM to the brain. Further supporting this, we found the leptin gene *LEP* to be the most prominently downregulated gene at both timepoints in exposures to A0 and A20. *LEP* is a regulator of KISS1 (Morelli et al., 2008), known to reduce odor-discrimination performance in mice by inhibiting neural activity in the OB (Sun et al., 2019). In addition, the downregulation of *LEP* upon urban PM exposure in OM cells has been previously shown (Chew et al., 2020). We also observed the upregulation of genes known to mediate inhibitory signal transduction. The gene *GAD1*, encoding glutamate decarboxylase 1, which is distinctly associated with the olfactory tract, was increased after 24-h exposure to A0 and A20. This enzyme converts glutamate to the inhibitory neurotransmitter GABA (Banerjee et al., 2013) and modulates GABA levels in the OB by odorant-induced synaptic activity-dependent regulation (Wang et al., 2017b). Excess GABA is known to reduce the activity of OB neurons (Gao et al., 2022). We found that 72-h exposure to A20 upregulated *GABRA3,* a GABA receptor involved in synaptic transmission in the OB (Banerjee et al., 2013; Mazurais et al., 2020). We thereby speculate that UFP-induced dysregulation of GABA signaling could impair olfactory signaling in the OM. Although a review by Wei et al. sums up well the current knowledge about mechanisms behind chemosensory dysfunction induced by environmental pollutants, exact molecular level alterations in olfactory signal transduction caused by external toxicants require further research (Wei et al., 2021). Taken together, these results suggest that exposure of primary human OM cells to A0 and A20 can impact key molecules involved in odorant signaling, and considering the important role of the OM in mediating information to the brain, further studies focusing on this aspect seem particularly interesting.

The integrity of any bodily epithelium is maintained by a carefully orchestrated network of different proteins forming TJ, adherens junctions (AJ), and actin filaments, which ties epithelium to the cytoskeleton (Belardi et al., 2020; Zihni et al., 2016). The appropriate stiffness of the ECM has also been demonstrated to be a critical determinant in the integrity of cell-cell junctions (Mammoto et al., 2013). Several studies have shown that diesel exhaust particles and $PM_{2.5}$ exposure compromise the human nasal epithelial barrier functions through decreased expression of TJ proteins, increased release of proinflammatory cytokines, and oxidative stress (Fukuoka et al., 2016; Ma et al., 2021; Xian et al., 2020; Zhao et al., 2018). Some studies suggest that gene-level alterations may be behind barrier dysfunction upon PM exposure (Fukuoka and Yoshimoto, 2018; Kim et al., 2020a; Song et al., 2020), but this has not previously been addressed in the human OM.

Our transcriptomic analyses revealed exposure-induced signs of compromised olfactory epithelial barrier integrity on several levels: downregulation of genes coding TJ-proteins, signs of dysregulation of genes coding structural proteins of the ECM and actin cytoskeleton, and lastly, strongly inhibited integrin signaling, which has a vital role in connecting the cell exterior to the interior. Thus far, the majority of air pollution studies assessing epithelial permeability have focused on the ZO-1 protein, which is indisputably a crucial player in maintaining epithelial integrity. In this study, RNA-Seq confirmed the OM cultures to express *ZO-1*, but it was not found to be differentially expressed upon UFP exposure. However, some other signature TJ protein-coding genes such as *CLDN1* and *OCLN* were downregulated following exposure to A20, and IPA results showed cellular pathways related to barrier integrity to be altered. Furthermore, UFP exposure resulted in decreased expression of several genes associated with epidermal barrier structure (*FLG*, keratins), with A20 eliciting a more severe impact than A0. These results are supported by existing literature, demonstrating that reduced expression of the gene *FLG* in cultured human nasal epithelial cells may

result in epithelial barrier dysfunction (Nakamura et al., 2021). Down-regulation of FLG has also been previously connected with exposure to PM (Kim et al., 2021; Song et al., 2020) and PAHs (Vogel et al., 2020). Considering the pivotal role of FLG and keratins in the assembly of the cytoskeleton as well as participating in building connections with adjacent cells and ECM (Yu et al., 2022), these findings suggest that UFP exposure may impair the keratin network formation in OM, therefore possibly affecting to barrier permeability. The most prominent Ingenuity pathways found at both timepoints with exposures to A0 and A20 were Actin Cytoskeleton Signaling, Signaling by Rho Family GTPases, and Integrin Signaling. Small GTPases, Rho and Rac have been shown to regulate VE-cadherin localization and cell–cell junctional integrity and therefore they are thought to be regulators of ECM stiffness affecting TJs and permeability in endothelial cells (Mammoto et al., 2013). Inhibited Pulmonary Fibrosis Idiopathic Signaling Pathway and dysregulation of collagen production might indicate disrupted ECM homeostasis which is a known hallmark of chronic obstructive pulmonary disease (COPD) (Liu et al., 2021). Since smoking and air pollution are known risk factors of COPD, we speculate that similar features could occur in OM upon exposure to UFPs. TJ formation and function are highly dependent on actin cytoskeleton dynamics which are also regulated by RHO GTPases (Zihni et al., 2016). $PM_{2.5}$ remarkably suppressed RHOA activity as well as actin reorganization in corneal epithelial cells (Cui et al., 2018). Overall, RHO GTPases seem to have a fundamental role as major regulators of barrier integrity via regulating both ECM stiffness and actin cytoskeleton dynamics (Mammoto et al., 2013; Zihni et al., 2016). These findings suggest that UFPs may impair the integrity of the barrier in OM cells by disrupting the dynamics of the ECM, as well as the actin cytoskeleton. In addition, integrin signaling was one of the most prominently inhibited pathways in both timepoints and exposures to A0 and A20. Integrins are transmembrane cell adhesion proteins participating in signal transduction and mediating cell adhesion to the ECM (Alberts et al., 2002). If epithelial cells lose connection with the ECM due to impaired integrin signaling, the machinery of cell death is initiated. A recent study reported inhibition of integrin signaling upon exposure to $PM_{2.5}$ in bronchial epithelial cells, assessed by metabolomics and proteomics approaches (Song et al., 2022). However, to date, the association of integrins with PM has not been elucidated in nasal/olfactory epithelial cells. Here, we are the first to report that integrin signaling is among the most suppressed pathways in primary human OM cells upon exposure to UFPs. Considering the essential role of integrins as a signal mediator as well as the regulator of cell adhesion, we speculate that integrins may have an eminent role in UFP-mediated dysfunction of the human OM.

Functional assessment of epithelial integrity with the TEER measurement corroborated the results of the transcriptomic data, showing that the most significant change in epithelial integrity was observed with exposure to A20 in both time points, while the effect of A0 was less pronounced. Euro6 was affected only slightly in TEER-values with the longer 72-h exposure time, which further supports the previous observations of Euro6 having only minor health effects on the OM cells. Collectively, our data provide vast new insights into the health impacts of UFP exhaust emission exposure, however, the study has some limitations. For instance, exposure to air pollutants in real life occurs throughout life, and exposure concentrations are usually relatively low. Mimicking this with in vitro model is challenging given that exposure time is quite limited and concentrations relatively high. Considering the time window of the cells in the laboratory, to reach the effect, which is cumulative over decades in real life, we need to use substantially rough treatment to cells to reach the same level of exposure. Cells are also more vulnerable when taken out from their natural environment, lacking sufficient clearance and defense mechanisms to fight external threats. However, here we used primary human cells, which on the other hand can bring more variation to the experimental data when compared to using commercially available cell lines but are also far more relevant than immortalized cell lines in terms of human exposures. It should also be noted that the procedures where particles are collected, extracted into liquid, and then dissolved again before their administration to cells, may change their physicochemical characteristics, altering their effects on cellular processes. However, using extracted particles with a high degree of physical and chemical characterization can provide important insight for deciphering cellular mechanisms responsible for adverse health outcomes associated with exposure. Although transcriptional differences may reveal us some molecular mechanisms, it doesn't necessarily translate into the next level(s). Further multi-omics studies, such as epigenetics and proteomics are needed to verify the identified DEGs and molecular mechanisms.

5. Conclusions

We provide evidence that the engine exhaust with state-of-the-art filtration and aftertreatments is less harmful to OM cells compared to a modern engine without filters. This difference might be emphasized with old technology engines. Euro6 exhaust caused only negligible changes, demonstrating the major impact of engine aftertreatment devices on adverse effects observed in human-derived OM cells *in vitro*. Instead, exposure to A0 and A20 caused substantial alterations in both the gene expression profile and function of OM cells. A20, the fossil diesel containing 20 % of aromatic content caused more severe and a broader spectrum of complications than the renewable diesel A0 used with the same engine. Elaborate effects were observed on the inflammatory response and xenobiotic metabolism, most likely due to the reactive nitrogen species and PAH contents of the emissions. Furthermore, hampered xenobiotic metabolism could be associated with disturbances in the clearance of chemical stimuli, possibly also affecting olfactory signaling. In addition, several processes known to regulate OM integrity were disrupted, indicating that the barrier might be compromised, and possibly leading to increased membrane permeability. Given that the OM can be a gateway of particles to the brain, we believe it is important to focus further research efforts to uncover how air pollutants exploit this path to the detriment of the brain. It is possible that UFPs might mediate the effects of harmful compounds, such as PAHs, on the brain through the olfactory route.

Supplementary data to this article can be found online at https://doi.org/10.1016/j.scitotenv.2023.167038.

CRediT authorship contribution statement

Laura Mussalo: Conceptualization, Investigation, Writing – original draft, Writing – review & editing, Visualization, Funding acquisition. **Simone Avesani:** Formal analysis, Resources, Visualization. **Muhammad Ali Shahbaz:** Investigation, Writing – review & editing. **Táňa Závodná:** Investigation. **Liudmila Saveleva:** Investigation, Writing – review & editing. **Anssi Järvinen:** Investigation, Resources, Writing – review & editing. **Riikka Lampinen:** Investigation, Writing – review & editing. **Irina Belaya:** Investigation, Writing – review & editing. **Zdeněk Krejčík:** Investigation. **Mariia Ivanova:** Investigation. **Henri Hakkarainen:** Investigation, Writing – review & editing. **Juho Kalapudas:** Resources. **Elina Penttilä:** Resources. **Heikki Löppönen:** Resources. **Anne M. Koivisto:** Resources. **Tarja Malm:** Conceptualization, Resources. **Jan Topinka:** Resources, Funding acquisition. **Rosalba Giugno:** Formal analysis, Funding acquisition. **Päivi Aakko-Saksa:** Resources, Writing – review & editing. **Sweelin Chew:** Conceptualization, Methodology, Investigation. **Topi Rönkkö:** Conceptualization, Writing – review & editing, Visualization. **Pasi Jalava:** Conceptualization, Writing – review & editing, Supervision, Project administration. **Katja M. Kanninen:** Conceptualization, Methodology, Writing – review & editing, Supervision, Project administration, Funding acquisition.

Declaration of competing interest

The authors declare the following financial interests/personal

relationships which may be considered as potential competing interests: Katja Kanninen reports financial support was provided by The Academy of Finland. Katja Kanninen reports financial support was provided by The Sigrid Juselius Foundation. Katja Kanninen reports financial support was provided by Horizon 2020 European Innovation Council Fast Track to Innovation. Tarja Malm reports financial support was provided by Horizon 2020 European Innovation Council Fast Track to Innovation. Pasi Jalava reports financial support was provided by Horizon 2020 European Innovation Council Fast Track to Innovation. Laura Mussalo reports financial support was provided by Kuopio Area Respiratory Foundation. Laura Mussalo reports financial support was provided by Finnish Brain Foundation. Laura Mussalo reports financial support was provided by Yrjö Jahnsson Foundation. Laura Mussalo reports financial support was provided by Päivikki and Sakari Sohlberg Foundation. Laura Mussalo reports financial support was provided by University of Eastern Finland.

Data availability

The data presented in this study are available on request from the corresponding author. RNA sequencing data are available from the European Genome-phenome Archive (EGA, https://ega-archive.org/) under the accession ID: EGAD00001011317.

Acknowledgment

This study was financially supported by The Academy of Finland (295425), The Sigrid Juselius Foundation, Kuopio Area Respiratory Foundation, The Finnish Brain Foundation, The Yrjö Jahnsson Foundation, Päivikki and Sakari Sohlberg Foundation, and by the University of Eastern Finland. This project has received funding from the European Union's Horizon 2020 research and innovation program under grant agreement No 814978.

References

Adams, D.R., Ajmani, G.S., Pun, V.C., Wroblewski, K.E., Kern, D.W., Schumm, L.P., McClintock, M.K., Suh, H.H., Pinto, J.M., 2016. Nitrogen dioxide pollution exposure is associated with olfactory dysfunction in older U.S. adults. Int Forum Allergy Rhinol 6, 1245–1252. https://doi.org/10.1002/alr.21829.

Agapite, J., Albou, L.P., Aleksander, S.A., Alexander, M., Anagnostopoulos, A.V., Antonazzo, G., Argasinska, J., Arnaboldi, V., Attrill, H., Becerra, A., Bello, S.M., Blake, J.A., Blodgett, O., Bradford, Y.M., Bult, C.J., Cain, S., Calvi, B.R., Carbon, S., Chan, J., Chen, W.J., Cherry, J.M., Cho, J., Christie, K.R., Crosby, M.A., Davis, P., da Veiga Beltrame, E., De Pons, J.L., D'Eustachio, P., Diamantakis, S., Dolan, M.E., dos Santos, G., Douglass, E., Dunn, B., Eagle, A., Ebert, D., Engel, S.R., Fashena, D., Foley, S., Frazer, K., Gao, S., Gibson, A.C., Gondwe, F., Goodman, J., Gramates, L.S., Grove, C.A., Hale, P., Harris, T., Hayman, G.T., Hill, D.P., Howe, D.G., Howe, K.L., Hu, Y., Jha, S., Kadin, J.A., Kaufman, T.C., Kalita, P., Karra, K., Kishore, R., Kwitek, A.E., Laulederkind, S.J.F., Lee, R., Longden, I., Luypaert, M., MacPherson, K. A., Martin, R., Marygold, S.J., Matthews, B., McAndrews, M.S., Millburn, G., Miyasato, S., Motenko, H., Moxon, S., Muller, H.M., Mungall, C.J., Muruganujan, A., Mushayahama, T., Nalabolu, H.S., Nash, R.S., Ng, P., Nuin, P., Paddock, H., Paulini, M., Perrimon, N., Pich, C., Quinton-Tulloch, M., Raciti, D., Ramachandran, S., Richardson, J.E., Gelbart, S.R., Ruzicka, L., Schaper, K., Schindelman, G., Shimoyama, M., Simison, M., Shaw, D.R., Shrivatsav, A., Singer, A., Skrzypek, M., Smith, C.M., Smith, C.L., Smith, J.R., Stein, L., Sternberg, P. W., Tabone, C.J., Thomas, P.D., Thorat, K., Thota, J., Toro, S., Tomczuk, M., Trovisco, V., Tutaj, M.A., Tutaj, M., Urbano, J.M., Van Auken, K., Van Slyke, C.E., Wang, Q., Wang, S.J., Weng, S., Westerfield, M., Williams, G., Wilming, L.G., Wong, E.D., Wright, A., Yook, K., Zarowiecki, M., Zhou, P., Zytkovicz, M., 2022. Harmonizing model organism data in the Alliance of Genome Resources. Genetics 220. https://doi.org/10.1093/GENETICS/IYAC022.

Ajmani, G.S., Suh, H.H., Pinto, J.M., 2016. Effects of ambient air pollution exposure on olfaction: a review. Environ. Health Perspect. 124, 1683–1693. https://doi.org/10.1289/EHP136.

Alberts, B., Johnson, A., Lewis, J., Raff, M., Roberts, K., Walter, P., 2002. Integrins, in: Molecular Biology of the Cell, 4th edition. Garland Science, New York.

Alves, C.A., Barbosa, C., Rocha, S., Calvo, A., Nunes, T., Cerqueira, M., Pio, C., Karanasiou, A., Querol, X., 2015. Elements and polycyclic aromatic hydrocarbons in exhaust particles emitted by light-duty vehicles. Environ. Sci. Pollut. Res. 11526–11542. https://doi.org/10.1007/s11356-015-4394-x.

Andrews, S., 2010. FastQC: A Quality Control Tool for High Throughput Sequence [WWW Document]. Online. URL. https://www.bioinformatics.babraham.ac.uk/projects/fastqc/.

Atoyan, R., Shander, D., Botchkareva, N. v, 2009. Non-neuronal expression of Transient Receptor Potential Type A1 (TRPA1) in human skin. J. Investig. Dermatol. 129, 2312–2315. https://doi.org/10.1038/jid.2009.58.

Banerjee, K., Akiba, Y., Baker, H., Cave, J.W., 2013. Epigenetic control of neurotransmitter expression in olfactory bulb interneurons. Int. J. Dev. Neurosci. 31, 415. https://doi.org/10.1016/J.IJDEVNEU.2012.11.009.

Belardi, B., Hamkins-Indik, T., Harris, A.R., Kim, J., Xu, K., Fletcher, D.A., 2020. A weak link with actin organizes tight junctions to control epithelial permeability. Dev. Cell 54, 792–804 e7. https://doi.org/10.1016/j.devcel.2020.07.022.

Bolger, A.M., Lohse, M., Usadel, B., 2014. Trimmomatic: a flexible trimmer for Illumina sequence data. Bioinformatics 30, 2114–2120. https://doi.org/10.1093/BIOINFORMATICS/BTU170.

Calderón-Garcidueñas, L., Stommel, E.W., Rajkumar, R.P., Mukherjee, P.S., Ayala, A., 2021. Particulate air pollution and risk of neuropsychiatric outcomes. What we breathe, swallow, and put on our skin matters. Int. J. Environ. Res. Publ. Health 18. https://doi.org/10.3390/ijerph182111568.

Cassee, F., Morawska, L., Peters, A., Wierzbicka, A., Buonanno, G., Cyrys, J., Schnelle-Kreis, J., Kowalski, M., Riediker, M., Birmili, W., Querol, X., Yildirim, A., Elder, A., Yu, I.J., Ovrevik, J., Hougaard, K., Loft, S., Schmid, O., Stoeger, T., Lucht, S., 2019. Ambient Ultrafine Particles: Evidence for Policy Makers. A Report Prepared by the 'Thinking Outside the Box' Team [WWW Document]. URL. https://efca.net/files/WHITE%20PAPER-UFP%20evidence%20for%20policy%20makers%20(25%20OCT).pdf (accessed 3.7.23).

Chang, Y., Siddens, L.K., Heine, L.K., Sampson, D.A., Yu, Z., Fischer, K.A., Löhr, C.V., Tilton, S.C., 2019. Comparative mechanisms of PAH toxicity by benzo[a]pyrene and dibenzo[def,p]chrysene in primary human bronchial epithelial cells cultured at air-liquid interface. Toxicol. Appl. Pharmacol. 379, 114644. https://doi.org/10.1016/J.TAAP.2019.114644.

Chen, C.R., Kachramanoglou, C., Li, D., Andrews, P., Choi, D., 2014. Anatomy and cellular constituents of the human olfactory mucosa: a review. J Neurol Surg B Skull Base 75, 293–300. https://doi.org/10.1055/s-0033-1361837.

Chen, J., Li, S.S., Fang, S.M., Zhang, Z., Yu, Q.Y., 2022. Olfactory dysfunction and potential mechanisms caused by volatile organophosphate dichlorvos in the silkworm as a model animal. J Hazard Mater 425. https://doi.org/10.1016/j.jhazmat.2021.127940.

Chew, S., Lampinen, R., Saveleva, L., Korhonen, P., Mikhailov, N., Grubman, A., Grubman, A., Grubman, A., Polo, J.M., Polo, J.M., Polo, J.M., Wilson, T., Komppula, M., Rönkkö, T., Gu, C., Mackay-Sim, A., Malm, T., White, A.R., Jalava, P., Kanninen, K.M., 2020. Urban air particulate matter induces mitochondrial dysfunction in human olfactory mucosal cells. Part. Fibre Toxicol. 17 https://doi.org/10.1186/s12989-020-00352-4.

Clifford, S., Mazaheri, M., Salimi, F., Ezz, W.N., Yeganeh, B., Low-Choy, S., Walker, K., Mengersen, K., Marks, G.B., Morawska, L., 2018. Effects of exposure to ambient ultrafine particles on respiratory health and systemic inflammation in children. Environ. Int. 114, 167–180. https://doi.org/10.1016/J.ENVINT.2018.02.019.

Costa, L.G., Cole, T.B., Dao, K., Chang, Y.C., Coburn, J., Garrick, J.M., 2020. Effects of air pollution on the nervous system and its possible role in neurodevelopmental and neurodegenerative disorders. Pharmacol. Ther. 210 https://doi.org/10.1016/j.pharmthera.2020.107523.

Couzens, M., Liu, M., Tüchler, C., Kofler, B., Nessler-Menardi, C., Parker, R.M.C., Klocker, H., Herzog, H., 2000. Peptide YY-2 (PYY2) and pancreatic polypeptide-2 (PPY2): species-specific evolution of novel members of the neuropeptide Y gene family. Genomics 64, 318–323. https://doi.org/10.1006/geno.2000.6132.

Cristaldi, A., Fiore, M., Oliveri Conti, G., Pulvirenti, E., Favara, C., Grasso, A., Copat, C., Ferrante, M., 2022. Possible association between PM2.5 and neurodegenerative diseases: a systematic review. Environ Res 208, 112581. https://doi.org/10.1016/j.envres.2021.112581.

Cui, Y.H., Hu, Z.X., Gao, Z.X., Song, X.L., Feng, Q.Y., Yang, G., Li, Z.J., Pan, H.W., 2018. Airborne particulate matter impairs corneal epithelial cells migration via disturbing FAK/RhoA signaling pathway and cytoskeleton organization. Nanotoxicology 12, 312–324. https://doi.org/10.1080/17435390.2018.1440651.

di Pizio, A., Behrens, M., Krautwurst, D., 2019. Beyond the flavour: the potential druggability of chemosensory G protein-coupled receptors. Int J Mol Sci 20. https://doi.org/10.3390/IJMS20061402.

Dobin, A., Davis, C.A., Schlesinger, F., Drenkow, J., Zaleski, C., Jha, S., Batut, P., Chaisson, M., Gingeras, T.R., 2013. STAR: ultrafast universal RNA-seq aligner. Bioinformatics 29, 15–21. https://doi.org/10.1093/BIOINFORMATICS/BTS635.

Doyle, K.L., Hort, Y.J., Herzog, H., Shine, J., 2012. Neuropeptide Y and peptide YY have distinct roles in adult mouse olfactory neurogenesis. J. Neurosci. Res. 90, 1126–1135. https://doi.org/10.1002/jnr.23008.

Durante, M.A., Kurtenbach, Stefan, Sargi, Z.B., Harbour, J.W., Choi, R., Kurtenbach, Sarah, Goss, G.M., Matsunami, H., Goldstein, B.J., 2020. Single-cell analysis of olfactory neurogenesis and differentiation in adult humans. Nat. Neurosci. 23, 323–326. https://doi.org/10.1038/s41593-020-0587-9.

Fischl, A.M., Heron, P.M., Stromberg, A.J., McClintock, T.S., 2014. Activity-dependent genes in mouse olfactory sensory neurons. Chem. Senses 39, 439. https://doi.org/10.1093/CHEMSE/BJU015.

Freeman, S.C., Karp, D.A., Kahwaji, C.I., 2021. Physiology, Nasal [WWW Document]. StatPearls. URL. https://www.ncbi.nlm.nih.gov/books/NBK526086/ (accessed 2.8.22).

Fukuoka, A., Yoshimoto, T., 2018. Barrier dysfunction in the nasal allergy. Allergol. Int. 67, 18–23. https://doi.org/10.1016/j.alit.2017.10.006.

Fukuoka, A., Matsushita, K., Morikawa, T., Takano, H., Yoshimoto, T., 2016. Diesel exhaust particles exacerbate allergic rhinitis in mice by disrupting the nasal epithelial barrier. Clin. Exp. Allergy 46, 142–152. https://doi.org/10.1111/cea.12597.

Fuzzi, S., Baltensperger, U., Carslaw, K., Decesari, S., Denier Van Der Gon, H., Facchini, M.C., Fowler, D., Koren, I., Langford, B., Lohmann, U., Nemitz, E., Pandis, S., Riipinen, I., Rudich, Y., Schaap, M., Slowik, J.G., Spracklen, D.v., Vignati, E., Wild, M., Williams, M., Gilardoni, S., 2015. Particulate matter, air quality and climate: lessons learned and future needs. Atmos. Chem. Phys. https://doi.org/10.5194/acp-15-8217-2015.

Gao, F., Gao, K., Zhang, P., Fu, Y., Liu, X., Bai, S., Li, W., Qian, Z., 2022. A biomimetic sensor using neurotransmitter detection to decode odor perception by an olfactory network. Biosens. Bioelectron. 211, 956–5663. https://doi.org/10.1016/j.bios.2022.114391.

Genter, M.B., Doty, R.L., 2019. Toxic exposures and the senses of taste and smell. Handb. Clin. Neurol. 164, 389–408. https://doi.org/10.1016/B978-0-444-63855-7.00022-8.

Grabacka, M., Pierzchalska, M., Płonka, P.M., Pierzchalski, P., 2021. The role of PPAR alpha in the modulation of innate immunity. Int. J. Mol. Sci. 22 https://doi.org/10.3390/IJMS221910545.

Hahad, O., Lelieveld, J., Birklein, F., Lieb, K., Daiber, A., Münzel, T., 2020. Ambient air pollution increases the risk of cerebrovascular and neuropsychiatric disorders through induction of inflammation and oxidative stress. Int. J. Mol. Sci. 21, 1–24. https://doi.org/10.3390/ijms21124306.

Hakkarainen, H., Järvinen, A., Lepistö, T., Salo, L., Kuittinen, N., Laakkonen, E., Yang, M., Martikainen, M.V., Saarikoski, S., Aurela, M., Barreira, L., Teinilä, K., Ihalainen, M., Aakko-Saksa, P., Timonen, H., Rönkkö, T., Jalava, P., 2023. Toxicity of exhaust emissions from high aromatic and non-aromatic diesel fuels using in vitro ALI exposure system. Sci. Total Environ. 890, 164215. https://doi.org/10.1016/J.SCITOTENV.2023.164215.

He, F., Wan, J., Chu, S., Li, X., Zong, W., Liu, R., 2022. Toxic mechanism on phenanthrene-triggered cell apoptosis, genotoxicity, immunotoxicity and activity changes of immunity protein in Eisenia fetida: combined analysis at cellular and molecular levels. Sci Total Environ 819. https://doi.org/10.1016/J.SCITOTENV.2022.153167.

Hochella, M.F., Mogk, D.W., Ranville, J., Allen, I.C., Luther, G.W., Marr, L.C., McGrail, B.P., Murayama, M., Qafoku, N.P., Rosso, K.M., Sahai, N., Schroeder, P.A., Vikesland, P., Westerhoff, P., Yang, Y., 2019. Natural, incidental, and engineered nanomaterials and their impacts on the earth system. Science 1979, 363. https://doi.org/10.1126/science.aau8299.

Huang, X.P., Karpiak, J., Kroeze, W.K., Zhu, H., Chen, X., Moy, S.S., Saddoris, K.A., Nikolova, V.D., Farrell, M.S., Wang, S., Mangano, T.J., Deshpande, D.A., Jiang, A., Penn, R.B., Jin, J., Koller, B.H., Kenakin, T., Shoichet, B.K., Roth, B.L., 2015. Allosteric ligands for the pharmacologically dark receptors GPR68 and GPR65. Nature 527, 477. https://doi.org/10.1038/NATURE15699.

Iaccarino, L., la Joie, R., Lesman-Segev, O.H., Lee, E., Hanna, L., Allen, I.E., Hillner, B.E., Siegel, B.A., Whitmer, R.A., Carrillo, M.C., Gatsonis, C., Rabinovici, G.D., 2021. Association between ambient air pollution and amyloid positron emission tomography positivity in older adults with cognitive impairment. JAMA Neurol. 78, 197–207. https://doi.org/10.1001/jamaneurol.2020.3962.

Imamura, F., Hasegawa-Ishii, S., 2016. Environmental toxicants-induced immune responses in the olfactory mucosa. Front. Immunol. 7, 475. https://doi.org/10.3389/FIMMU.2016.00475.

Jankowska-Kieltyka, M., Roman, A., Nalepa, I., 2021. The air we breathe: air pollution as a prevalent proinflammatory stimulus contributing to neurodegeneration. Front Cell Neurosci. https://doi.org/10.3389/fncel.2021.647643.

Jeong, J., Bae, S. Yong, Choi, J., 2021. Identification of toxicity pathway of diesel particulate matter using AOP of PPARγ inactivation leading to pulmonary fibrosis. Environ. Int. 147 https://doi.org/10.1016/J.ENVINT.2020.106339.

Jew, K., Herr, D., Wong, C., Kennell, A., Morris-Schaffer, K., Oberdörster, G., O'Banion, M.K., Cory-Slechta, D.A., Elder, A., 2019. Selective memory and behavioral alterations after ambient ultrafine particulate matter exposure in aged 3xTgAD Alzheimer's disease mice. Part Fibre Toxicol 16. https://doi.org/10.1186/s12989-019-0323-3.

Jia, H., Liu, Y., Guo, D., He, W., Zhao, L., Xia, S., 2021. PM2.5-induced pulmonary inflammation via activating of the NLRP3/caspase-1 signaling pathway. Environ Toxicol 36, 298. https://doi.org/10.1002/TOX.23035.

Kaarthik, J., Keshava, C., Richardson, D.L., Weston, A., Nath, J., 2009. Immune response signatures of benzo(α)pyrene exposure in normal human mammary epithelial cells in the absence or presence of chlorophyllin. Cancer Genomics Proteomics 6, 1–12.

Kang, D., Jung, I.B., Lee, S.Y., Park, S.J., Kwon, S.J., Park, D.H., Son, J.W., 2020. Particulate matter less than 10 μm (PM 10) activates cancer related genes in lung epithelial cells. Inhal. Toxicol. 32, 487–493. https://doi.org/10.1080/08958378.2020.1850936.

Kanninen, K.M., Lampinen, R., Rantanen, L.M., Odendaal, L., Jalava, P., Chew, S., White, A.R., 2020. Olfactory cell cultures to investigate health effects of air pollution exposure: implications for neurodegeneration. Neurochem. Int. 136 https://doi.org/10.1016/j.neuint.2020.104729.

Kim, Y., Lim, K.-M., 2021. Skin barrier dysfunction and filaggrin. Arch. Pharm. Res. 44, 36–48. https://doi.org/10.1007/s12272-021-01305-x.

Kim, K.-H., Jahan, S.A., Kabir, E., Brown, R.J.C., 2013. A review of airborne polycyclic aromatic hydrocarbons (PAHs) and their human health effects. Environ. Int. 60, 71–80. https://doi.org/10.1016/j.envint.2013.07.019.

Kim, H.S., Kim, H.J., Kim, N., Song, J.J., Son, B.S., Yang, J.H., Lee, C.M., Park, M.K., Seo, Y.R., 2020a. Toxicogenomic study to identify potential signaling alterations related to nasal inflammatory damages induced by diesel exhaust particles in primary human nasal epithelial cells. Toxicol. In Vitro 69. https://doi.org/10.1016/j.tiv.2020.104994.

Kim, S.J., Kim, N., Park, S.H., Kim, H.S., Song, J.J., Son, B.S., Jang, A.S., Park, M.K., Seo, Y.R., 2020b. Genomic approach to explore altered signaling networks of olfaction in response to diesel exhaust particles in mice. Sci Rep 10. https://doi.org/10.1038/s41598-020-74109-6.

Kim, B.E., Kim, J., Goleva, E., Berdyshev, E., Lee, J., Vang, K.A., Lee, U.H., Han, S.Y., Leung, S., Hall, C.F., Kim, N.R., Bronova, I., Lee, E.J., Yang, H.R., Leung, D.Y.M., Ahn, K., 2021. Particulate matter causes skin barrier dysfunction. JCI Insight 6. https://doi.org/10.1172/JCI.INSIGHT.145185.

Krämer, A., Green, J., Pollard, J., Tugendreich, S., 2014. Causal analysis approaches in ingenuity pathway analysis. Bioinformatics 30, 523–530. https://doi.org/10.1093/BIOINFORMATICS/BTT703.

Kwon, H.S., Ryu, M.H., Carlsten, C., 2020. Ultrafine particles: unique physicochemical properties relevant to health and disease. Exp. Mol. Med. 52, 318–328. https://doi.org/10.1038/s12276-020-0405-1.

Lampinen, R., Fazaludeen, M.F., Avesani, S., Örd, T., Penttilä, E., Lehtola, J.M., Saari, T., Hannonen, S., Saveleva, L., Kaartinen, E., Acosta, F.F., Cruz-Haces, M., Löppönen, H., Mackay-Sim, A., Kaikkonen, M.U., Koivisto, A.M., Malm, T., White, A.R., Giugno, R., Chew, S., Kanninen, K.M., 2022. Single-cell RNA-Seq analysis of olfactory mucosal cells of Alzheimer's disease patients. Cells 11, 676. https://doi.org/10.3390/CELLS11040676.

Le Bihanic, F., Morin, B., Cousin, X., Le Menach, K., Budzinski, H., Cachot, J., 2014. Developmental toxicity of PAH mixtures in fish early life stages. Part I: adverse effects in rainbow trout. Environ. Sci. Pollut. Res. 21, 13720–13731. https://doi.org/10.1007/s11356-014-2804-0.

Li, J., Zhang, Y., Zhang, L., An, Z., Song, J., Wang, C., Ma, Y., Gu, Q., Luo, Q., Yang, W., Du, Y., Wu, W., 2021. Fine particulate matter exposure exacerbated nasal mucosal damage in allergic rhinitis mice via NLRP3 mediated pyroptosis. Ecotoxicol. Environ. Saf. 228, 112998. https://doi.org/10.1016/j.ecoenv.2021.112998.

Liao, Y., Smyth, G.K., Shi, W., 2014. featureCounts: an efficient general purpose program for assigning sequence reads to genomic features. Bioinformatics 30, 923–930. https://doi.org/10.1093/BIOINFORMATICS/BTT656.

Liu, G., Philp, A.M., Corte, T., Travis, M.A., Schilter, H., Hansbro, N.G., Burns, C.J., Eapen, M.S., Sohal, S.S., Burgess, J.K., Hansbro, P.M., 2021. Therapeutic targets in lung tissue remodelling and fibrosis. Pharmacol. Ther. 225 https://doi.org/10.1016/j.pharmthera.2021.107839.

Love, M.I., Huber, W., Anders, S., 2014. Moderated estimation of fold change and dispersion for RNA-seq data with DESeq2. Genome Biol. 15 https://doi.org/10.1186/S13059-014-0550-8.

Luoma, K., Niemi, J.v., Aurela, M., Lun Fung, P., Helin, A., Hussein, T., Kangas, L., Kousa, A., Rönkkö, T., Timonen, H., Virkkula, A., Petäjä, T., 2021. Spatiotemporal variation and trends in equivalent black carbon in the Helsinki metropolitan area in Finland. Atmos. Chem. Phys. 21, 1173–1189. https://doi.org/10.5194/ACP-21-1173-2021.

Ma, S., Xian, M., Wang, Y., Wang, C., Zhang, L., 2021. Budesonide repairs decreased barrier integrity of eosinophilic nasal polyp epithelial cells caused by PM2.5. Clin. Transl. Allergy 11, e12019. https://doi.org/10.1002/clt2.12029.

Maher, B.A., Ahmed, I.A.M., Karloukovski, V., MacLaren, D.A., Foulds, P.G., Allsop, D., Mann, D.M.A., Torres-Jardón, R., Calderon-Garciduenas, L., 2016. Magnetite pollution nanoparticles in the human brain. Proc. Natl. Acad. Sci. U. S. A. 113, 10797–10801. https://doi.org/10.1073/pnas.1605941113.

Mammoto, A., Mammoto, T., Kanapathipillai, M., Yung, C.W., Jiang, E., Jiang, A., Lofgren, K., Gee, E.P.S., Ingber, D.E., 2013. Control of lung vascular permeability and endotoxin-induced pulmonary oedema by changes in extracellular matrix mechanics. Nat. Commun. 4, 1–10. https://doi.org/10.1038/ncomms2774, 2013 4: 1.

Mazurais, D., Servili, A., Le Bayon, N., Gislard, S., Madec, Lauriane, Zambonino-Infante, J.-L., 2020. Long-term exposure to near-future ocean acidification does not affect the expression of neurogenesis- and synaptic transmission-related genes in the olfactory bulb of European sea bass (Dicentrarchus labrax). J. Comp. Physiol. B 190, 161–167. https://doi.org/10.1007/s00360-019-01256-2.

Mazzarella, G., Ferraraccio, F., Prati, M.v., Annunziata, S., Bianco, A., Mezzogiorno, A., Liguori, G., Angelillo, I.F., Cazzola, M., 2007. Effects of diesel exhaust particles on human lung epithelial cells: an in vitro study. Respir. Med. 101, 1155–1162. https://doi.org/10.1016/j.rmed.2006.11.011.

Merleev, A.A., Le, S.T., Alexanian, C., Toussi, A., Xie, Y., Marusina, A.I., Watkins, S.M., Patel, F., Billi, A.C., Wiedemann, J., Izumiya, Y., Kumar, A., Uppala, R., Michelle Kahlenberg, J., Liu, F.T., Adamopoulos, I.E., Wang, E.A., Ma, C., Cheng, M.Y., Xiong, H., Kirane, A., Luxardi, G., Andersen, B., Tsoi, L.C., Lebrilla, C.B., Gudjonsson, J.E., Maverakis, E., 2022. Biogeographic and disease-specific alterations in epidermal lipid composition and single-cell analysis of acral keratinocytes. JCI Insight 7. https://doi.org/10.1172/JCI.INSIGHT.159762.

Mills, E.G., Yang, L., Abbara, A., Dhillo, W.S., Comninos, A.N., 2022. Current perspectives on kisspeptins role in behaviour. Front Endocrinol (Lausanne) 13. https://doi.org/10.3389/FENDO.2022.928143.

Morelli, A., Marini, M., Mancina, R., Luconi, M., Vignozzi, L., Fibbi, B., Filippi, S., Pezzatini, A., Forti, G., Vannelli, G.B., Maggi, M., 2008. Sex steroids and leptin regulate the "first kiss" (KiSS 1/g-protein-coupled receptor 54 system) in human gonadotropin-releasing-hormone-secreting neuroblasts. J. Sexual Med. 5, 1097–1113. https://doi.org/10.1111/j.1743-6109.2008.00782.x.

Morinaka, S., Nakamura, H., 2000. Inflammatory cells in nasal mucosa and nasal polyps. Auris Nasus Larynx 27.

Nakamura, M., Kamiya, K., Furuhata, A., 1#, K.I., Niyonsaba, F., 2021. S100A7 co-localization and up-regulation of filaggrin in human sinonasal epithelial cells. Curr Med Sci 41, 863–868. https://doi.org/10.1007/s11596-021-2431-1.

Nazarenko, Y., Pal, D., Ariya, P.A., 2021. Air quality standards for the concentration of particulate matter 2.5, global descriptive analysis. Bull. World Health Organ. 99, 125–137. https://doi.org/10.2471/BLT.19.245704.

Neste Renewable Diesel Handbook [WWW Document]. URL. https://www.neste.com/sites/default/files/attachments/neste_renewable_diesel_handbook.pdf (accessed 8.16.23).
Nieder, R., Benbi, D.K., 2022. Reactive nitrogen compounds and their influence on human health: an overview. Rev. Environ. Health 37, 229–246. https://doi.org/10.1515/REVEH-2021-0021/ASSET/GRAPHIC/J_REVEH-2021-0021_FIG_006.JPG.
Nold-Petry, C.A., Nold, M.F., Zepp, J.A., Kim, S.H., Voelkel, N.F., Dinarello, C.A., 2009. IL-32–dependent effects of IL-1β on endothelial cell functions. Proc. Natl. Acad. Sci. U. S. A. 106, 3883. https://doi.org/10.1073/PNAS.0813334106.
Ogino, K., Zhang, R., Takahashi, H., Takemoto, K., Kubo, M., Murakami, I., Wang, D.H., Fujikura, Y., 2014. Allergic airway inflammation by nasal inoculation of particulate matter (PM2.5) in NC/Nga mice. PLoS One 9. https://doi.org/10.1371/JOURNAL.PONE.0092710.
QIAGEN Inc. Ingenuity Pathway Analysis | QIAGEN Digital Insights [WWW Document]. n.d. URL. https://digitalinsights.qiagen.com/products-overview/discovery-insights-portfolio/analysis-and-visualization/qiagen-ipa/ (accessed 3.6.23).
Rönkkö, T., Timonen, H., 2019. Overview of sources and characteristics of nanoparticles in urban traffic-influenced areas. J. Alzheimers Dis. 72, 15–28. https://doi.org/10.3233/JAD-190170.
Saarikoski, S., Järvinen, A., Markkula, L., Aurela, M., Kuittinen, N., Barreira, L., Aakko-Saksa, P., Timonen, H., Jalava, P., Rönkkö, T., n.d. Impact of Fuels and novel engine and exhaust aftertreatment technologies on pollutants and their potential to form secondary aerosols of modern passenger cars. (Unpublished results).
Sammeta, N., McClintock, T.S., 2010. Chemical stress induces the unfolded protein response in olfactory sensory neurons. J. Comp. Neurol. 518, 1825. https://doi.org/10.1002/CNE.22305.
Schraufnagel, D.E., 2020. The health effects of ultrafine particles. Exp. Mol. Med. 52, 311–317. https://doi.org/10.1038/s12276-020-0403-3.
Schwartz, M., Menetrier, F., Heydel, J.-M., Chavanne, E., Faure, P., Labrousse, M., Lirussi, F., Canon, F., Mannervik, B., Briand, L., Neiers, F., 2020. Interactions between odorants and glutathione transferases in the human olfactory cleft. Chem. Senses 45, 645–654. https://doi.org/10.1093/chemse/bjaa055.
Sima, M., Cervena, T., Elzeinova, F., Ambroz, A., Beranek, V., Vojtisek-Lom, M., Klema, J., Ciganek, M., Rossner, P., 2022. The Impact of Extractable Organic Matter From Gasoline and Alternative Fuel Emissions on Bronchial Cell Models (BEAS-2B, MucilAirTM). https://doi.org/10.1016/j.tiv.2022.105316.
Song, C., Liu, L., Chen, J., Hu, Y., Li, J., Wang, B., Bellusci, S., Chen, C., Dong, N., 2020. Evidence for the critical role of the PI3K signaling pathway in particulate matter-induced dysregulation of the inflammatory mediators COX-2/PGE 2 and the associated epithelial barrier protein Filaggrin in the bronchial epithelium. Cell Biol. Toxicol. 36, 301–313. https://doi.org/10.1007/S10565-019-09508-1.
Song, X., Liu, J., Geng, N., Shan, Y., Zhang, B., Zhao, B., Ni, Y., Liang, Z., Chen, J., Zhang, L., Zhang, Y., 2022. Multi-omics analysis to reveal disorders of cell metabolism and integrin signaling pathways induced by PM 2.5. J Hazard Mater 424. https://doi.org/10.1016/j.jhazmat.2021.127573.
Steiner, S., Bisig, C., Petri-Fink, A., Rothen-Rutishauser, B., 2016. Diesel exhaust: current knowledge of adverse effects and underlying cellular mechanisms. Arch. Toxicol. 90, 1541–1553. https://doi.org/10.1007/S00204-016-1736-5.
Sun, C., Tang, K., Wu, J., Xu, H., Zhang, W., Cao, T., Zhou, Y., Yu, T., Li, A., 2019. Leptin modulates olfactory discrimination and neural activity in the olfactory bulb. Acta Physiol. 227 https://doi.org/10.1111/apha.13319.
Sunderman, F.W.J., 2001. Nasal toxicity, carcinogenicity, and olfactory uptake of metals. Ann. Clin. Lab. Sci. 31, 3–24.
Tomazic, P.V., Birner-Gruenberger, R., Leitner, A., Obrist, B., Spoerk, S., Lang-Loidolt, D., 2014. Nasal mucus proteomic changes reflect altered immune responses and epithelial permeability in patients with allergic rhinitis. J. Allergy Clin. Immunol. 133, 741–750. https://doi.org/10.1016/j.jaci.2013.09.040.
Vogel, C.F.A., Van Winkle, L.S., Esser, C., Haarmann-Stemmann, T., 2020. The aryl hydrocarbon receptor as a target of environmental stressors - implications for pollution mediated stress and inflammatory responses. Redox Biol 34. https://doi.org/10.1016/J.REDOX.2020.101530.
Vondracek, J., Pencikova, K., Neca, J., Ciganek, M., Grycov, A., Dvorak, Z., Machala, M., 2017. Assessment of the aryl hydrocarbon receptor-mediated activities of polycyclic aromatic hydrocarbons in a human cell-based reporter gene assay. Environ. Pollut. 220, 307–316. https://doi.org/10.1016/j.envpol.2016.09.064.
Wang, C., Yang, J., Zhu, L., Yan, L., Lu, D., Zhang, Q., Zhao, M., Li, Z., 2017a. Never deem lightly the "less harmful" low-molecular-weight PAH, NPAH, and OPAH — disturbance of the immune response at real environmental levels. Chemosphere 168, 568–577. https://doi.org/10.1016/j.chemosphere.2016.11.024.
Wang, M., Cai, E., Fujiwara, N., Fones, L., Brown, E., Yanagawa, Y., Cave, J.W., 2017b. Odorant sensory input modulates DNA secondary structure formation and heterogeneous ribonucleoprotein recruitment on the tyrosine hydroxylase and glutamic acid decarboxylase 1 promoters in the olfactory bulb. J. Neurosci. 37, 4778–4789. https://doi.org/10.1523/JNEUROSCI.1363-16.2017.
Watson, J.D., Prokopec, S.D., Smith, A.B., Okey, A.B., Pohjanvirta, R., Boutros, P.C., 2013. TCDD Dysregulation of 13 AHR-Target Genes in Rat Liver. https://doi.org/10.1016/j.taap.2013.12.004.
Wei, S., Xu, T., Jiang, T., Yin, D., 2021. Chemosensory dysfunction induced by environmental pollutants and its potential as a novel neurotoxicological indicator: a review. Environ. Sci. Technol. 55, 10911–10922. https://doi.org/10.1021/ACS.EST.1C02048/ASSET/IMAGES/MEDIUM/ES1C02048_0003.GIF.
Werner, S., Nies, E., 2018. Olfactory dysfunction revisited: a reappraisal of work-related olfactory dysfunction caused by chemicals. J Occup Med Toxicol 13. https://doi.org/10.1186/S12995-018-0209-6.
Wihersaari, H., Pirjola, L., Karjalainen, P., Saukko, E., Kuuluvainen, H., Kulmala, K., Keskinen, J., Rönkkö, T., 2020. Particulate emissions of a modern diesel passenger car under laboratory and real-world transient driving conditions. Environ. Pollut. 265 https://doi.org/10.1016/J.ENVPOL.2020.114948.
World Health Organization, 2021. WHO Global Air Quality Guidelines: Particulate Matter (PM2.5 and PM10), Ozone, Nitrogen Dioxide, Sulfur Dioxide and Carbon Monoxide [WWW Document]. URL. https://apps.who.int/iris/handle/10665/345329 (accessed 2.8.22).
World Health Organization. Regional Office for Europe, 2000. Air Quality Guidelines for Europe Second Edition [WWW Document]. URL. https://apps.who.int/iris/handle/10665/107335 (accessed 2.27.23).
Xian, M., Ma, S., Wang, K., Lou, H., Wang, Y., Zhang, L., Wang, C., Akdis, C.A., 2020. Particulate matter 2.5 causes deficiency in barrier integrity in human nasal epithelial cells. Allergy Asthma Immunol Res 12, 56–71. https://doi.org/10.4168/aair.2020.12.1.56.
Xu, H., Ou, L., Li, Y., Hawkins, T.R., Wang, M., 2022. Life cycle greenhouse gas emissions of biodiesel and renewable diesel production in the United States. Environ. Sci. Technol. 56, 7512–7521. https://doi.org/10.1021/ACS.EST.2C00289.
Yu, B., Kong, D., Cheng, C., Xiang, D., Cao, L., Liu, Y., He, Y., 2022. Assembly and recognition of keratins: a structural perspective. Semin. Cell Dev. Biol. 128, 1084–9521. https://doi.org/10.1016/j.semcdb.2021.09.018.
Zarcone, M.C., Duistermaat, E., van Schadewijk, A., Jedynska, A., Hiemstra, P.S., Kooter, I.M., 2016. Cellular response of mucociliary differentiated primary bronchial epithelial cells to diesel exhaust. Am. J. Physiol. Lung Cell. Mol. Physiol. 311, L111–L123. https://doi.org/10.1152/ajplung.00064.2016.
Zhang, Y., Dong, S., Wang, H., Tao, S., Kiyama, R., 2016. Biological impact of environmental polycyclic aromatic hydrocarbons (ePAHs) as endocrine disruptors *. Environ. Pollut. 213, 809–824. https://doi.org/10.1016/j.envpol.2016.03.050.
Zhang, L., Yang, L., Zhou, Q., Zhang, X., Xing, W., Wei, Y., Hu, M., Zhao, L., Toriba, A., Hayakawa, K., Tang, N., 2019. Size distribution of particulate polycyclic aromatic hydrocarbons in fresh combustion smoke and ambient air: a review ScienceDirect. J. Environ. Sci. 88, 370–384. https://doi.org/10.1016/j.jes.2019.09.007.
Zhang, Q., Meng, X., Shi, S., Kan, L., Chen, R., Kan, H., 2022. Overview of particulate air pollution and human health in China: evidence, challenges, and opportunities. Innovation 3. https://doi.org/10.1016/J.XINN.2022.100312.
Zhao, R., Guo, Z., Zhang, R., Deng, C., Xu, J., Dong, W., Hong, Z., Yu, H., Situ, H., Liu, C., Zhuang, G., 2018. Nasal epithelial barrier disruption by particulate matter ≤2.5 μm via tight junction protein degradation. J. Appl. Toxicol. 38, 678–687. https://doi.org/10.1002/jat.3573.
Zihni, C., Mills, C., Matter, K., Balda, M.S., 2016. Tight junctions: from simple barriers to multifunctional molecular gates. Nat. Rev. Mol. Cell Biol. 17, 564–580. https://doi.org/10.1038/nrm.2016.80, 2016 17:9.
Zundel, C.G., Ryan, P., Brokamp, C., Heeter, A., Huang, Y., Strawn, J.R., Marusak, H.A., 2022. Air pollution, depressive and anxiety disorders, and brain effects: a systematic review. Neurotoxicology. https://doi.org/10.1016/j.neuro.2022.10.011.